



Contents lists available at ScienceDirect

Physics of the Earth and Planetary Interiors

journal homepage: www.elsevier.com/locate/pepi



Geomagnetic secular variation in the Cretaceous Normal Superchron and in the Jurassic

Andrew J. Biggin^{a,*}, Douwe J.J. van Hinsbergen^{a,b}, Cor G. Langereis^a,
Gijs B. Straathof^{a,b,1}, Martijn H.L. Deenen^a

^a Paleomagnetic Laboratory 'Fort Hoofddijk', Utrecht University, Budapestlaan 17, 3584 CD Utrecht, The Netherlands

^b Department of Geology, University of Leicester, University Road, LE1 7RH Leicester, UK

ARTICLE INFO

Article history:

Received 5 February 2008

Received in revised form 4 July 2008

Accepted 5 July 2008

Keywords:

Geomagnetic field

Palaeomagnetism

Secular variation

Cretaceous

Jurassic

Superchron

ABSTRACT

It is now widely thought that geomagnetic polarity reversals occur spontaneously as a result of normal dynamo action rather than being externally triggered. If this is the case, then it may well be that periods of time in which the geomagnetic reversal frequency was dramatically different were characterised by different styles of secular variation. Two such periods were the Cretaceous Normal Superchron (CNS: 84–125 Ma) when the field was dominantly of a single polarity for 40 Myr and the Jurassic period (145–200 Ma) when reversals occurred at an average rate of as much as 4.6 Myr^{-1} . Here, we analyse a database of new and published palaeomagnetic directions from lavas emplaced during these periods in order to obtain first-order descriptions of the palaeosecular variation (PSV) during these times. We then compare these records with one another and with that produced for the period 0–5 Ma (with average reversal frequency of 4.0 Myr^{-1}). Our results are more equivocal than those obtained in a previous similar study [McFadden, P.L., Merrill, R.T., McElhinny, M.W., Lee, S.H., 1991. Reversals of the Earth's magnetic-field and temporal variations of the dynamo families. *Journal of Geophysical Research-Solid Earth and Planets* 96, 3923–3933]. We demonstrate that this is probably a result of the previous study being affected by an artefact of their correction for within-site scatter. The usefulness of our Jurassic record is severely limited by the restricted palaeolatitude span of the available data. However, our record for the CNS is sufficient to allow us to conclude that it was likely that secular variation then was different from that in the 0–5 Ma period. This supports the hypothesis of a link between PSV and reversal frequency and therefore endorses PSV analysis as a first-order tool for determining geomagnetic stability in the past.

© 2008 Elsevier B.V. All rights reserved.

1. Introduction

The secular variation (SV) of the geomagnetic field is the variation (on timescales of hundreds to thousands of years) that arises internally from the dynamo action which is responsible for generating the field. Numerical models of the geodynamo (e.g. Glatzmaier and Roberts, 1995) which exhibit SV may also spontaneously exhibit more dramatic 'excursions' and full polarity reversals similar to those observed in the palaeomagnetic record. Partly as a result of these simulations, it is now widely thought that excursions and reversal transitions are natural outgrowths of SV (Gubbins, 1999) and not externally triggered by, e.g. boundary layer instabilities as has been previously considered (e.g. McFadden and Merrill, 1993).

Magnetostratigraphy has provided unambiguous evidence that the propensity of the geomagnetic field to reverse its polarity has varied over timescales of 10^7 – 10^8 years (e.g. Opdyke and Channell, 1996). These are much longer than the timescales typically associated with the core and are likely forced through mantle processes changing the total heat flux across the core–mantle boundary and/or its lateral distribution (Gubbins, 1994). Numerous attempts have been made to tie in these variations in reversal frequency to observations of the long-term average geomagnetic palaeointensity (e.g. Biggin and Thomas, 2003; Prevot et al., 1990; Tarduno et al., 2001; Tarduno et al., 2002; Tauxe and Staudigel, 2004; Thomas et al., 2000) as well as geological processes observed at the Earth's surface (e.g. Courtillot and Olson, 2007; Larson and Olson, 1991). If reversals are intrinsic outgrowths of 'normal' SV then we may expect that records of palaeosecular variation (PSV) should also display such long timescale variations in keeping with changes in mean reversal frequency. This study aims to test this hypothesis using new data and a different analytical approach to that used by McFadden et al. (1991).

* Corresponding author. Tel.: +31 30 253 5246.

E-mail address: biggin@geo.uu.nl (A.J. Biggin).

¹ Now at: School of Geosciences, Grant Institute, West Mains Road, University of Edinburgh, UK.

Palaeomagnetic records from sedimentary sections (e.g. [Tauxe and Hartl, 1997](#)) can provide continuous full-vector records of PSV. However, all but the most rapidly deposited sediments will tend to average out the variation to some degree that may be difficult to quantify. Conversely, palaeomagnetic directions measured from lava samples provide an essentially instantaneous spot reading of the geomagnetic field. This, together with the fact that the ‘within-site statistics’ measurable from lavas allows correction for measurement errors implies that lavas provide potentially more reliable data for statistical analyses of PSV than do sedimentary rocks. One potential drawback of palaeosecular variation of lavas (PSVL) studies is that rapid bursts of volcanic activity can result in under-representation of PSV (e.g. [Knight et al., 2004](#)). However, this potential problem can be detected by careful analysis of the data (see Section 2 of this study).

PSV analyses are most commonly performed by taking virtual geomagnetic poles (VGPs) from numerous lavas and plotting their angular dispersion against the (palaeo)latitude of the source rocks on a VGP dispersion curve. [McFadden et al. \(1991\)](#) reported clear and significant differences in VGP dispersion curves from time periods within the last 195 Myr with different average reversal frequencies. In particular, they found that during times of low reversal frequency, VGP dispersion tended to be lower at low palaeolatitudes than during times of higher reversal frequencies and also that this dispersion increased much more with increasing palaeo-latitude in the former than in the latter periods. These observations imply that normal SV is intrinsically linked to reversal frequency and also suggest that PSVL can be used as a tool, independent of magnetostratigraphy, to ascertain dynamo stability at other times in Earth’s history.

[McFadden et al.’s](#) findings were based on a database compiled 25 years ago ([Lee, 1983](#)) which was split up into bins based on the palaeolatitude and age of the VGPs. No details of the individual studies providing the data were given and more recent PSVL studies have cast doubt on the reliability of some of the findings. In addition to reporting a detailed full-vector palaeomagnetic analysis of mid-Cretaceous Arctic lavas, [Tarduno et al. \(2002\)](#) produced a VGP dispersion curve for the Cretaceous Normal Superchron and found that it was not as steep as that observed for the same period by [McFadden et al.](#) This difference was probably, at least partly, a result of the more recent study using far more exacting selection criteria than the earlier work. The present study supersedes the PSV analysis of [Tarduno et al.](#) because we use a substantially larger over-

all dataset and pay special attention to the within-site statistics of these data.

Very recently, [Johnson et al. \(2008\)](#) performed the most detailed and rigorous PSVL study yet using data from lavas formed in the last 5 Myr. Their data was unquestionably more reliable than that available to previous studies of the same period (e.g. [McElhinny and McFadden, 1997](#); [McFadden et al., 1988](#)) and, interestingly, it produced a VGP dispersion curve that was significantly flatter in shape than the curves the older studies had produced. Furthermore, they demonstrated using simulated data that latitudinal dependence of VGP dispersion can be introduced as an artefact of poor quality data.

The Glatzmaier–Roberts numerical geodynamo model ([Glatzmaier et al., 1999](#)) operating in different stability regimes produces VGP dispersion curves with different shapes ([Fig. 1](#)). Specifically, the mean VGP dispersion curve produced by their highly stable ‘superchron-like’ Model E is lower than that produced by their Model G which has a reversal frequency closer to the present-day field. Furthermore, there is a broad tendency for the standard deviation of the VGP dispersion (shown in [Fig. 1](#) as error bars) to increase with its mean value. Consequently, the Model E curve shown in [Fig. 1a](#) indicates that the pattern of PSV (as defined by VGP dispersion produced by sites positioned along a complete circle of latitude) was less variable in time than that for Model G.

In this study, we will use the PSVL technique to examine if SV is different in periods of dramatically different reversal frequency. Such a connection is suggested by numerical models and the empirical study of [McFadden et al. \(1991\)](#), and might also be intuitively expected.

In Section 2, we present the analytical techniques we used in this study and in Section 3 we look in detail at the effects that low quality data can have on a PSVL study. This will serve the purpose of guiding future studies.

In Section 4, we will introduce the datasets that were used in this analysis. These were taken from rocks from a total of 11 localities emplaced in the CNS and rocks from 17 localities from the Jurassic period. These two periods were chosen because the analysis of [McFadden et al. \(1991\)](#) found that data in the time windows 80–120 and 120–195 Ma displayed PSV behaviour at the extreme ends of the spectrum of behaviour they observed across the entire period 0–195 Ma.

There is some controversy over the precise date of the onset of the CNS (see e.g. [Gong et al., 2008](#) for a discussion) but we will take

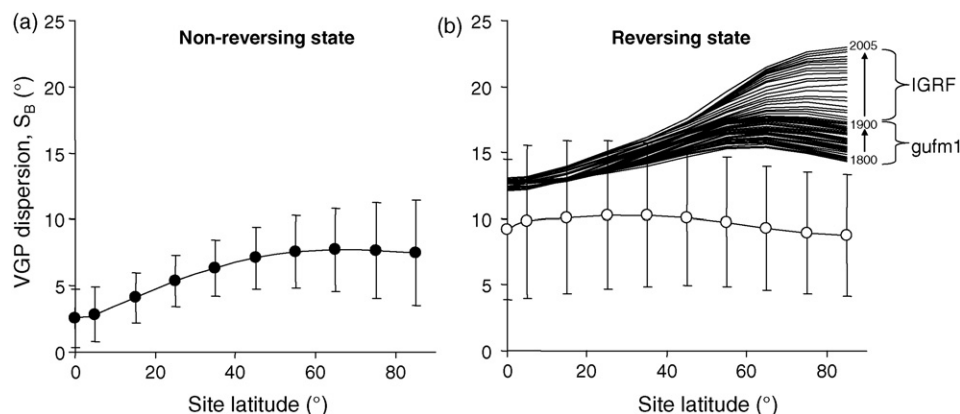


Fig. 1. Comparison of VGP dispersion curves (averaged for N and S hemispheres) produced by numerical simulations of the geodynamo. The reversing (non-reversing) state relates to Model G (Model E) of [Glatzmaier et al. \(1999\)](#). A total of 20 kyr of model time was used to produce the curves and at each time step (48 years for Model G, 95 years for Model E), an ‘instantaneous’ VGP dispersion curve was calculated using 72 ‘sites’ spaced every 5° of longitude along a line of latitude. The circles are the average of these instantaneous curves and the error bars represent the standard deviation. The lines in (b) are individual ‘instantaneous’ VGP dispersion curves plotted from the *gufm1* model (1800–1900; [Jackson et al., 2000](#)) and the International Geomagnetic Reference Field (IGRF; 1900–2005).

here the period 84–125 Ma defined by [Gradstein et al. \(2004\)](#). The superchron (C34n in the geomagnetic polarity timescale) may contain up to three brief reversed sub-chrons ([Ogg and Smith, 2004](#)) implying a maximum reversal frequency of 0.15 Myr^{-1} . The average reversal frequency for the Jurassic period (145–200 Ma) is less well constrained since the period denoted by chrons M25–M36 suggest many more reversals in the deep tow (MMA, marine magnetic anomaly) record than are indicated in magnetostratigraphic outcrop sections. If each of the inferred reversals in the MMA record is accepted then the average frequency across the whole period is 4.6 Myr^{-1} but this value could be reduced to as low as 3.1 Myr^{-1} if only reversals evident in the outcrop sections are to be trusted. It should also be noted that our knowledge of the reversal record during the period 190–200 Ma is rather poorly constrained ([Ogg, 2004](#)).

In Section 5, we compare the VGP dispersion curves produced by the data from the CNS and Jurassic period and in Section 6, we compare these curves with the Johnson et al. curve for the last 5 Myr and discuss all of our findings.

2. Methodology

We group palaeomagnetic data into *datasets*, each one of which consists of a collection of N VGPs from rocks of similar age and from the same geographic region (frequently the same formation). Each one of these VGPs is produced from a single palaeomagnetic sampling site equating to a single rock unit (lava, tuff, or high-level intrusion) and we are interested in using their angular dispersion as a measure of PSV. This dispersion will be partly caused by the geomagnetic secular variation, and partly by random errors associated with the sampling and measuring process. It is desirable to remove the latter source of dispersion so that the accuracy of the estimate of the dispersion caused by the SV is improved. The angular dispersion of VGPs from N units due to SV (S_B) is calculated thus:

$$S_B = \left[\frac{1}{N-1} \sum_{i=1}^N \left(\Delta_i^2 - \frac{S_{Wi}^2}{n_i} \right) \right]^{1/2} \quad (i = 1, \dots, N) \quad (1)$$

where Δ_i gives the angular distance of the i th VGP from the geographic pole or mean VGP. S_{Wi} is the within-site dispersion associated with each VGP which must be estimated from the scatter observed between the n_i individual sample directions. S_{Wi} and n_i will be abbreviated to S_W and n from hereon. To calculate S_W , first the known estimate of the precision parameter, k is (approximately) translated from direction to pole-space using Eq. (2) from [Cox \(1970\)](#) which makes the reasonable assumption of a Fisherian distribution ([Fisher, 1953](#)) of within-site directions:

$$K = k \left(\frac{1}{8} (5 + 18 \sin^2 \lambda + 9 \sin^4 \lambda) \right)^{-1} \quad (2)$$

where λ is the palaeolatitude of the sampling site and K and k are the within-site precision parameters of the distribution in pole and direction space respectively. The within-site dispersion is then approximated by

$$S_W = \frac{81}{\sqrt{K}} \quad (3)$$

Regardless of whether or not geomagnetic excursions and reversal transitions are purely outgrowths of 'normal' SV, their presence in a complete description of the time-averaged field is warranted. That said, the proportion of time the field spends in such a state is rather small and measurements of S_B are strongly influenced by 'outlier' VGPs (because it is sensitive to Δ_i^2). Therefore, we consider it desirable to exclude definitely excursions data (as well as out-

liers produced by measurement or recording errors) and to focus on the dispersion of VGPs produced by the field undergoing SV away from times of excursions and reversals. To do this, it is necessary to apply some threshold for Δ_i of VGPs in a dataset. There are two common approaches to obtaining this maximum cutoff value and both will be employed here. The first is to apply some arbitrary fixed cutoff value; when we employ this approach, we choose 45° as this is intermediate between the extremes chosen by previous studies and is also the value chosen by [Johnson et al. \(2008\)](#) for their analysis of the 0–5 Ma period. The second is to make the (reasonable) assumption that the distribution of VGPs is Fisherian and to use the iterative process defined by [Vandamme \(1994\)](#) to obtain an optimum cutoff angle, variable with palaeolatitude, from the dataset itself.

Some PSVL studies (e.g. [McFadden et al., 1991](#)) use plate reconstructions to relocate palaeomagnetic sampling sites to their position at the time the lavas were emplaced. The value of Δ_i in Eq. (1) is then calculated as the angular distance of the VGP from the 'geographic' pole. However, these plate reconstructions may themselves be based largely on the results of palaeomagnetic studies or else on the doubtful ([Tarduno et al., 2003](#)) fixed hotspot assumption. Therefore, in this study, we prefer to use the palaeomagnetic data to define the geographic pole directly based on the geocentric axial dipole (GAD) assumption. We therefore take the mean of the VGPs from the N sites in a dataset as the geographic pole and measure Δ_i from this mean pole. We also use the inclination of the mean direction to obtain our measurement of λ , the palaeolatitude of the dataset. The accuracy of this approach for different sizes of datasets (i.e. different values of N) is examined in Section 3.2.

Implicit to the study of PSV using measurements of VGP dispersion is the assumption that the geomagnetic field activity is sufficiently represented in the datasets. This requires a sufficiently large dataset of VGPs spanning a sufficient length of time (ideally at least several tens or hundreds of thousands of years, [Merrill and McFadden, 2003](#)). A potential problem of using data from lavas is that they can be emplaced in rapid bursts of volcanic activity which last only a short amount of time. A symptom of a sequence of lavas under-representing PSV is that the VGP positions from each flow display some serial correlation as the directions tracked the drift of the geomagnetic pole. However, while a lack of serial correlation in a large dataset implies that PSV must be well represented, the converse is not true: the presence of serial correlation, particularly in a large dataset, does not make an under-representation of the time-averaged field indubitable.

In the present study, it was deemed useful to have some quantitative non-parametric test for serial correlation in our datasets. For this we introduce a Non-Random-Ordering (NRO) factor which is calculated as follows:

1. Input the dataset of palaeomagnetic directions in stratigraphic order if known.
2. Calculate the angular distance $\Delta_{i(i+1)}$ between the palaeomagnetic direction of each flow and its successor.
3. Sum these to produce $\Sigma \Delta_{i(i+1)}$.
4. Randomise the order of the magnetic directions and repeat steps 2 and 3.
5. Repeat step 4 10,000 times and rank the values of $\Sigma \Delta_{i(i+1)}$ produced.

The position of the original $\Sigma \Delta_{i(i+1)}$ amongst the 10,000 randomised values is then indicative of the degree of ordering in the original dataset. Specifically, its rank divided by 10,000 is the *NRO factor* we will use which is the probability of this order being non-random. Consequently, the serial correlation is significant at the

95% confidence level if the NRO factor exceeds 0.95. This is essentially the same procedure for detecting serial correlation as that outlined by Watson and Beran (1967) but does not require the assumption that the $\Sigma \Delta_{i(i+1)}$ values are normally distributed.

The NRO factor is equally effective at detecting clusters of similar magnetic directions as it is at detecting progressive serial correlation. This is useful because many palaeomagnetic studies do not provide an explicit stratigraphy but do group sites by sampling localities which may produce related directions. In this study, by inputting the data in an order which reflects the geographic distribution of the sampling sites, it was still possible to provide some test for potential under-representation of SV in several of the studies which did not provide an explicit stratigraphic relationship.

The NRO factor should, in most cases, indicate where bursts of extrusive activity could lead to the over-representation of short periods of SV. However, in this study we only seek to identify this problem and discuss its significance and not to correct for it. Very similar directions from consecutive lavas are sometimes averaged by researchers (e.g. Knight et al., 2004) but this is not something that we will subject either our own or other published data to in this study. The reasons for this are, firstly, that there is no objective way of determining precisely how similar two or more directions should be in order that they are averaged, and secondly that, as will be explained in Section 4.2, it is largely unnecessary for the purposes of this study. This notwithstanding, future palaeomagnetic studies should of course always design their sampling strategy with the aim of maximising the likelihood of averaging SV.

The phenomenological Model G of McFadden et al. (1988) is used to describe the shapes of VGP dispersion curves. This model describes S_B as a function of (palaeo)latitude (λ) using two shape parameters a and b :

$$S_B = \sqrt{a^2 + (b\lambda)^2} \quad (4)$$

In this study, the values of a and b are chosen to minimise the sum of the squares of the deviation of the curve from the data. Model G was produced based on observations of the recent field (IGRF65); the a parameter is argued to represent variations in the equatorially asymmetric spherical harmonic terms of the field and the b parameter represents variations in the equatorially symmetric terms. We use it in this study to allow comparisons to be made with the results of McFadden et al. (1991).

For the plots where we bin the S_B data from the datasets by palaeolatitude, we will also use the same approach as McFadden et al. (1991) where the mean dispersion S_λ of a bin is given by

$$S_\lambda = \bar{S}_B = \left[\frac{\sum S_B^2(N-1)}{(\sum N) - 1} \right]^{1/2} \quad (5)$$

and its palaeolatitude is the simple arithmetic mean of the binned datasets.

In Sections 3 and 6, we will use simulated datasets to test various different aspects of the PSVL analysis. These datasets are all generated in the same way.

1. A number N of VGPs are randomly generated from a Fisher distribution with mean position at the geographic north pole and with precision parameter K calculated (Eq. (3)) from the 'true' (input) angular dispersion, S_B .
2. Each of these VGPs is converted into a corresponding direction at latitude λ .
3. Each one of these then forms the centre of a Fisher distribution (in direction space) with (input) precision parameter κ from which n directions can be drawn at random from.

The resulting simulated dataset realistically combines the dispersion due to both secular variation and within-site random errors.

3. The potential for bias in PSVL studies

3.1. The effects of n and k on VGP dispersions

The conclusions of PSV studies may potentially be strongly biased by the quality of data used in the analysis. Johnson et al. (2008) provided evidence that the strong latitudinal dependence of VGP dispersion observed from lavas of the last 5 Myr by McElhinny and McFadden (1997) may, at least in part, be an artefact of the low technical quality of the data that were used.

Since the conversion of magnetic directions into VGPs uses the (palaeo)latitude of the sampling site, latitudinally independent within-site dispersion of mean directions will translate directly into a latitudinal-dependent dispersion of VGPs. The S_W correction built into Eq. (1) can remove this artefact but to work properly it requires that n , the number of samples used to produce the mean direction, is sufficiently large so that the estimated precision parameter, k is a good estimate for the actual precision parameter, κ .

In Fig. 2, we show the results of several simulations of PSV studies. In all cases, the dispersion of VGPs due to geomagnetic SV is Fisherian, constant with latitude and 15° . All the deviations from $S_B = 15^\circ$ are entirely due to artefacts introduced by the measuring process. A number of interesting observations can be made from these plots. Fig. 2a shows that a large amount of within-site scatter coupled with no S_W correction being applied causes a strong positive latitudinal dependence of VGP dispersion to be introduced. This is largely removed if one incorporates the S_W correction but, because the k values of the site mean directions are poorly constrained by the low n , this introduces its own artefact (in this case a weak negative latitudinal dependence of VGP dispersion on latitude). Applying a minimum criterion for the apparent k value produces an artefact intermediate between the two described above.

Fig. 2b shows that a dataset with high n but low κ can still produce a positive latitudinal dependence of VGP dispersion if a S_W correction is not applied. However, since the k values are now well constrained, the S_W correction now works reasonably well. Fig. 2c and d indicates that low within-site errors, even when coupled to a low n and not corrected for, do not lead to significant artefacts being introduced.

When the data used in the present study (see Section 4) are combined, the total number ΣN of site mean directions from lavas where k was likely to be well-defined (i.e. those with $n \geq 5$) was 498. The median k value for these mean directions was 182. Consequently, we choose $\kappa = 182$ for the rest of the simulations we will discuss in this section so that they are directly applicable to our analyses of VGP dispersion in the CNS and the Jurassic.

This study will employ two sets of data. Group 1 includes only our 'high quality' data with $n \geq 5$ and $k \geq 50$. Fig. 3a and b shows that, when $N = 1000$, the application of the within-site error correction to such data produces an estimate for S_B that is within 1° of the true value. Consequently, we expect Group 1 datasets to introduce no bias through low n and/or k effects (low N effects will be discussed shortly).

Group 2 will be used to verify observations made from the Group 1 datasets. It will have the advantage of including more data (increasing both N and the number of datasets available) but will include datasets with lower n and k values than those in Group 1. Most significantly, some of these datasets will be from sites with $n = 1$. For $n < 5$, the k value becomes an unreliable measure of κ and for $n = 1$, there can be no estimate at all of how precise the

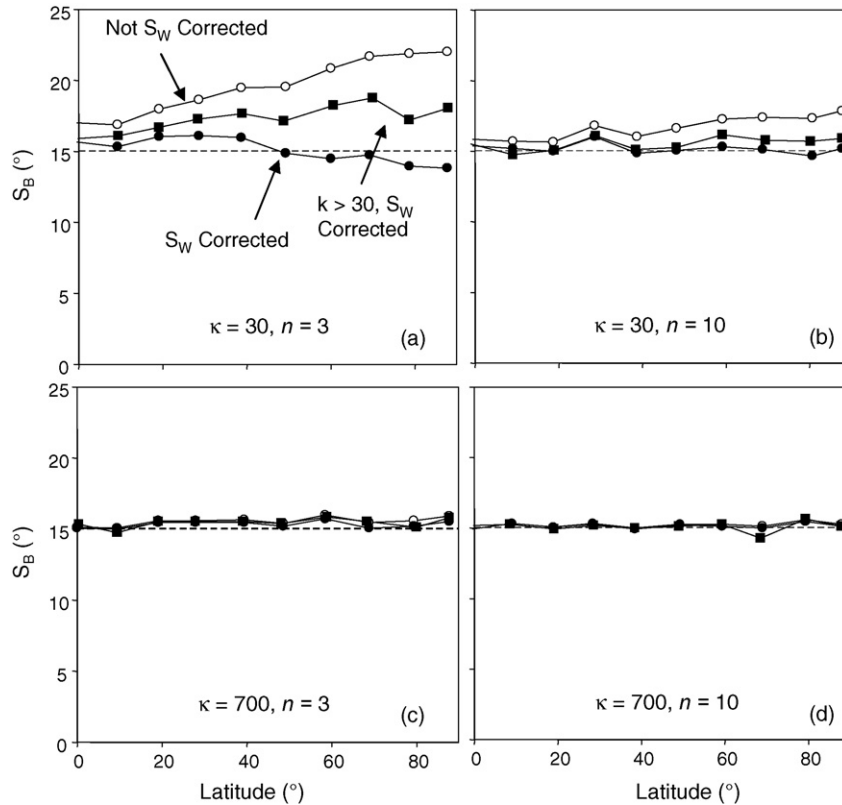


Fig. 2. Tests for artefacts introduced by measurement of a VGP dispersion curve using simulated data. The number of simulated sites (N) at each latitude was 1000 in all plots. Extreme values of the within-site precision parameter (κ) and number of specimens per site (n) were chosen to show the full range of behaviour. In all cases, the geomagnetic variation produces Fisher-distributed VGPs with $S_B = 15^\circ$ at all latitudes (dashed line in figures). Deviations from this line are purely a product of simulated measurement errors. No VGP cutoff was applied.

measurement is. Nonetheless, this data can still be useful if it is dealt with carefully. If we chose to apply no within-site scatter correction to these results, then we could expect to introduce some significant artefacts to our results, especially if the real S_B is low. Fig. 3c and d illustrates this and also shows the effects of ‘guessing’ the κ value for datasets with $n = 1$. If one guesses it correctly, the S_W correction is reasonably effective and so long as the κ value is not underestimated, the situation is improved over that of not applying any S_W correction (shown by the $k_{est} = \infty$ curve). If the within-site scatter of the directions is assumed to be higher than it actually is (i.e. if k is assumed to be much lower than κ actually is), then the S_W correction can severely bias the measured value of S_B to low values (shown by the $k_{est} = 50$ curve).

The plots shown in Fig. 3c and d have significant implications for PSV studies which generate estimates for S_B using data from sedimentary rocks (e.g. Cronin et al., 2001; Kruiver et al., 2000). Since such studies are generally based on measurements of only 1 sample per stratigraphic level, no estimate of S_W (the amount of random errors associated with the measurement process) is available and therefore no correction is made for this. This is equivalent to taking the $k = \infty$ curve in Fig. 3c and d which, as shown, can lead to S_B being significantly overestimated particularly if its true value is low. Future studies of this type should apply some ‘within-site’ dispersion correction to help reduce this problem. Even if this dispersion is entirely unknown (i.e. if there is only one sample per stratigraphic level), an arbitrarily large assumed value of k (e.g. 600), will at least represent some improvement over the current assumed k value of infinity.

We wished to test the effects of applying a fixed S_W correction based on $k = 182$ to all of the data used in this study with $n < 5$.

The distribution of k values observed in those site mean directions used in this study with $n \geq 5$ can be very well approximated with a log-normal distribution (Fig. 4a). We generated 10,000 synthetic values at random from such a distribution (Fig. 4b) and used these as κ values for the same number of synthetic mean directions from 10 different palaeolatitudes. Fig. 4c and d shows the VGP dispersion curves we would expect to observe given $S_B = 5^\circ$ and $S_B = 15^\circ$ if we applied a S_W correction (assuming a κ value of 182 for all sites) and if we did not. This S_W correction acts to bring the dispersion curve much closer to the expected value in both cases. Consequently, based on the reasonable assumption that the distribution of κ values in our sites with $n < 5$ is similar to that in our sites with $n \geq 5$, the application of a fixed S_W correction based on $k = 182$ in all sites should work reasonably well. We therefore apply this correction to our Group 2 data with $n < 5$.

3.2. The effects of N on measured VGP dispersion

The largest constraint on effective measurement of VGP dispersion curves through geological time is the number of reliable site mean data available for them. This is especially the case for the present study because, unlike McFadden et al. (1991) who used plate tectonic reconstructions, we rely on the palaeomagnetic data itself (specifically the mean inclination) to define the palaeolatitude of each dataset.

We investigated the effects of different values of N (the number of site means per dataset) on a simulated analysis of PSV by drawing 10 synthetic datasets of N site mean directions for each latitude (Fig. 5). As one would expect, the range of values measured for the palaeolatitude and S_B is much larger when N is smaller. When

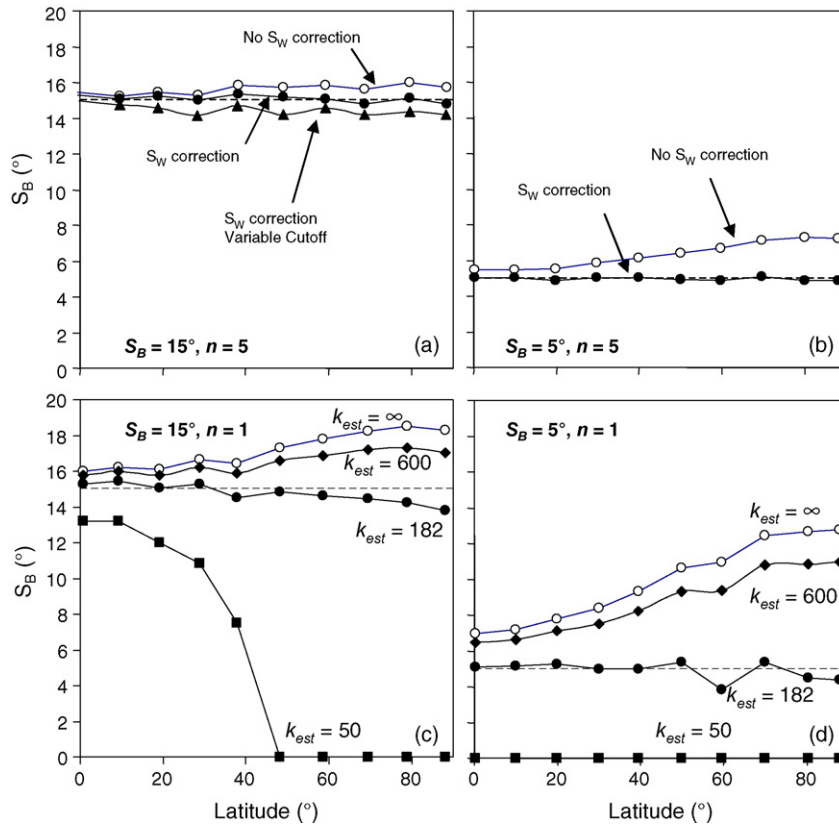


Fig. 3. More tests for artefacts introduced by measurement of a VGP dispersion curve using simulated data. $N = 1000$ at all latitudes and the within-site precision parameter (κ) of the simulated data was 182. Unless stated otherwise, a VGP cutoff of 45° was applied. In plots (a) and (b), the within-site correction was based on the measured estimate (k) of the precision parameter. In plots (c) and (d), the correction was based on a ‘guess’ of the k value (k_{est}) as indicated.

the true value of S_B is 15° and $N = 5$, the inaccuracies introduced into measurements of both S_B and palaeolatitude are so large as to make the results of any single measurement essentially useless. Furthermore, the uncertainty limits produced for these estimates are also not reliable for $N < 18$ (see values of $\Delta 95$ in Fig. 5).

As we might expect the amplitude of the noise produced by the low N effects is proportional to the actual (geomagnetic) value of S_B . This is demonstrated in the final panel of Fig. 5 where a simulated dispersion of $S_B = 5^\circ$ with $N = 5$ is shown for comparison with the other plots which have $S_B = 15^\circ$.

In this study, the paucity of data (particularly those that meet Group 1 criteria in the Jurassic period) is such that we were required to retain datasets with $N < 18$ and even to use a few datasets with $N < 10$. In the latter case, we do not consider their estimates of S_B , in themselves, to be reliable and therefore we employ them only in an indicative sense.

4. Sources of data

4.1. Data from lower Cretaceous lavas of the Gobi Altai

This study was initiated as a consequence of a large dataset of site mean directions from Mongolian lavas from the Gobi Altai region for the CNS becoming available (Hankard et al., 2005, 2007; van Hinsbergen et al., 2008). In this paper, we present new data from 68 lavas from the Gobi Altai (Table A1), which were specifically sampled for a PSV study. Fourteen lavas were sampled with two samples each in section Jaran Bogd, in addition to 16 lava sites with $n = 7$, already reported earlier in van Hinsbergen et al. (2008). Moreover, 54 consecutive lavas were sampled with one sample each in a ~ 1 km thick volcanic stratigraphy in section Kharaat Uul,

southeast of Mt. Arz Bogd. For exact locations, age details, demagnetisation procedures and rock magnetic properties we refer to van Hinsbergen et al. (2008). The directions used here are corrected for bedding tilt, which amounts $5\text{--}10^\circ$. Table 1 and Fig. 6 summarises the Gobi Altai lava data for the CNS; all directions that were not clearly lightening-induced remagnetisations are included.

The data are split into two groups based on the mean inclination of the directions. Sites from the Southeast Artz Bogd region (which we will term the SEAB group) display clearly steeper inclinations ($\sim 8^\circ$) than those from the rest (which we term non-SEAB). This is extremely unlikely to reflect a difference in palaeolatitude (of $\sim 10^\circ$) between the two groups. The Gobi Altai lavas (apart from the SEAB) display indistinguishable mean directions from one another which strongly suggests that the region was at polar standstill for the period during which they were emplaced (95–125 Ma; Hankard et al., 2007; van Hinsbergen et al., 2008). van Hinsbergen et al. (2008) presented two possible explanations for the discrepancy of the SEAB directions. The first is that the directions do not adequately sample the variation of the geomagnetic field and therefore overrepresent a particular spell of PSV. The second is that these particular lavas were not emplaced horizontally and that, in making a bedding plane correction to the measured directions of remanence, an artificially steep inclination was introduced.

Several observations made in this study make it appear that the second explanation given above is the more likely. The full SEAB dataset has a larger VGP dispersion than that of the non-SEAB dataset (Tables 1 and 3). Furthermore, there is strong evidence for serial correlation of directions in only a small proportion of the SEAB lavas (the seven lavas of the Khatavch which were sampled with more than one core are the only ones with NRO factor > 0.95 ; Table 1). Consequently, we retain the SEAB data for the PSV analysis

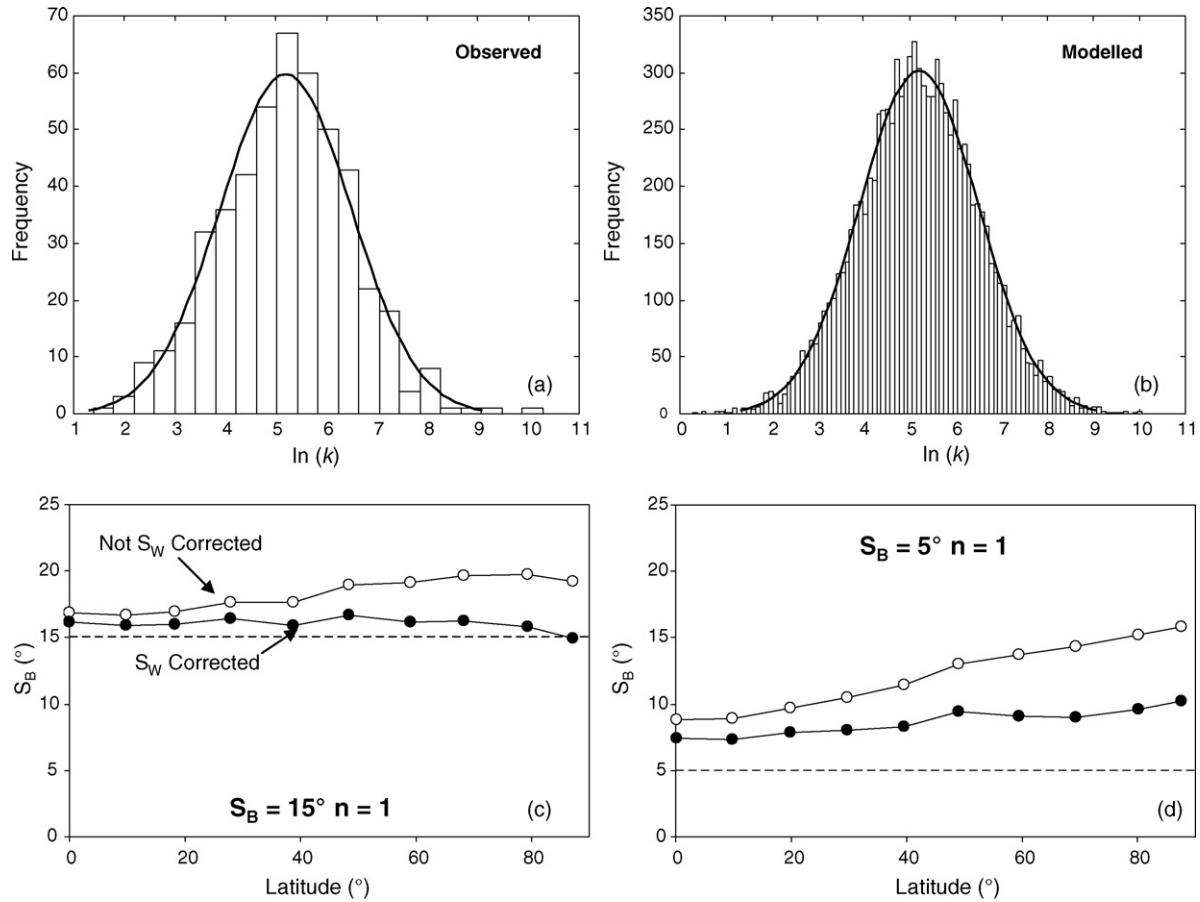


Fig. 4. (a) Log-distribution of k values observed for site means used in this study with $n \geq 5$. A normal curve is overlain (b) 10,000 random picks from a distribution modelled on that observed in (a). (c and d) Simulated VGP dispersion curves ($N=1000$ at all latitudes) produced using site mean data with $n=1$ and k drawn randomly from the distribution shown in (b). A 45° VGP cutoff was used.

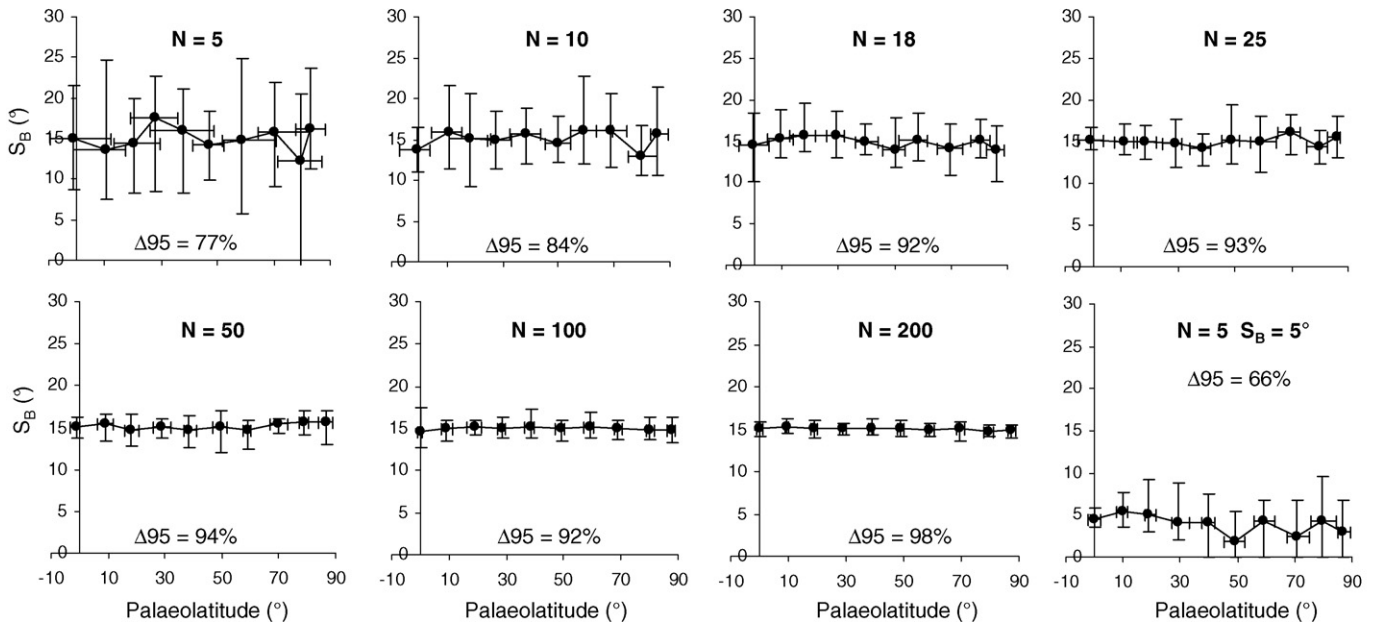


Fig. 5. Simulated VGP dispersion curves showing the degree of noise introduced by having different values of N (number of sites at each latitude). Plotted points are the average of 10 separate simulations and the error bars show the full range of the ten values. The simulated geomagnetic scatter was 15° in the first seven panels and the individual sites had $n=5$ and $\kappa=182$. No VGP cutoff was applied. Note that a lower geomagnetic dispersion (last panel) results in less noise being produced (for a given value of N). $\Delta 95$ is the percentage of the S_B estimates which are within their associated 95% uncertainty limits (obtained using the bootstrap approach) of the true value.

Table 1
Data from the Gobi Altai basalts used in this study

| Group | Locality | Age (Ma) | Refs. | Lat (°N) | Long (°E) | Dec (°) | Inc (°) | <i>N</i> | <i>k</i> | α_{95}° | NRO factor |
|----------|----------------------------|-------------|------------|----------|-----------|---------|---------|----------|----------|-----------------------|------------|
| SEAB | Kharaat Uul Single Samples | 115.4–119.3 | This study | 44.3 | 102.7 | 37.4 | 68.3 | 54 | 42.9 | 3.1 | 0.84 |
| SEAB | Tsagaan Tsav | 115.4–119.3 | vH08 | 44.4 | 102.4 | 13.8 | 75.3 | 10 | 122.2 | 4.4 | 0.88 |
| SEAB | Kharaat Uul Multi-samples | 115.4–119.3 | vH08 | 44.4 | 102.6 | 18.4 | 73.6 | 9 | 60.3 | 6.7 | 0.41 |
| SEAB | Khatavch | 115.4–119.3 | vH08 | 44.3 | 102.4 | 355.8 | 71.2 | 7 | 597.8 | 2.5 | 0.98 |
| non-SEAB | Jaran Bogd multi-samples | 118.2–124.3 | vH08 | 44.8 | 100.7 | 6.4 | 60.6 | 16 | 54.0 | 5.2 | 0.99* |
| non-SEAB | Jaran Bogd 2-samples | 118.2–124.3 | This study | 44.8 | 100.7 | 13.5 | 59.1 | 14 | 57.2 | 6.4 | 0.26 |
| non-SEAB | Dulaan Bogd | 118.2–124.3 | vH08 | 44.9 | 101.0 | 12.7 | 59.5 | 7 | 87.6 | 6.5 | |
| non-SEAB | Baga Bogd | 122.7–124.7 | vH08 | 44.8 | 101.8 | 14.9 | 59.7 | 7 | 64.3 | 7.6 | 0.72 |
| non-SEAB | Bulgantii Uul | 122.7–124.7 | vH08 | 44.8 | 102.0 | 19.5 | 63.2 | 11 | 27.7 | 8.8 | 0.95* |
| non-SEAB | Bulgantii North | 122.7–124.7 | vH08 | 44.8 | 102.0 | 13.8 | 63.1 | 7 | 35.4 | 10.3 | 0.83 |
| non-SEAB | Khalzan Khairkhan | 122.7–124.7 | vH08 | 44.7 | 102.1 | 353.2 | 72.5 | 6 | 57.5 | 8.9 | 0.99 |
| non-SEAB | Tsost | 94.7–107 | vH08 | 44.3 | 102.2 | 6.5 | 66.2 | 7 | 41.7 | 9.5 | 0.34 |
| non-SEAB | Artz Bogd | 94.7–107 | H05 | 44.3 | 102.2 | 12.4 | 66.1 | 30 | 53.2 | 3.9 | 0.99 |
| non-SEAB | Shovon/Khurmen Uul | 94.7–107 | H05, H07 | 44.4 | 103.8 | 10.2 | 61.9 | 24 | 50.6 | 4.4 | 0.52 |
| SEAB | All | 115.4–119.3 | | | | 29.6 | 70.6 | 80 | 44.9 | 2.5 | |
| non-SEAB | All | 94.7–124.7 | | | | 11.4 | 62.8 | 129 | 49.6 | 1.9 | |

Refs.: vH08 = van Hinsbergen et al. (2008); H05 = Hankard et al. (2005); H07 = Hankard et al. (2007). Where several profiles existed within the same locality, the lowest NRO factor (where $N \geq 5$) is given. The asterisk indicates that sedimentary layers had formed between some of the lavas included in the marked profile.

(Section 5), but modify its palaeolatitude so that it is equal to that of the non-SEAB dataset.

In the non-SEAB dataset, the NRO factor is highly significant for several localities (Table 1) including two of those (Jaran Bogd and Bulgantii Uul) where sedimentary layers were found between individual lavas. This is similar to the observation made by Knight et al. (2004) for Moroccan lavas from the Central Atlantic Magmatic Province (CAMP) and suggests very rapid deposition of the sedimentary horizons. However, the mean directions from the majority of non-SEAB localities are highly consistent (Fig. 6a) despite them being erupted in pulses of volcanism (see van Hinsbergen et al., 2008 for more details) which together spanned a period of more than 30 Myr. This strongly suggests that data from most of the localities largely average the PSV regardless of whether they exhibit serial correlation. One locality (Khalzan Khairkhan) has a mean

direction slightly away from the rest as well as NRO factor of 0.99; these data likely do not average PSV on their own but may be combined with the rest.

4.2. Data from the literature

We searched the global palaeomagnetic database (GPMDB; <http://www.ngu.no/dragon/Palmag/paleomag.htm>) and the recent literature for suitable data for analysing PSV in the CNS and in the Jurassic period. Our criteria were

1. Data from lavas and welded tuffs, with an age range entirely within the CNS (84–125 Ma) or the Jurassic (145–200 Ma). A few data from non-welded tuffs and dykes were also included (Tables 2 and 3)—the reliability of the estimates of S_B which are derived from these will be discussed in the next section.
2. Every manuscript was checked and the data were excluded if there were any suspicion of the directions not being primary or affected by uncertain post-emplacement tilting.
3. The samples must have undergone stepwise demagnetisation to isolate the characteristic remanence. This corresponds to the directions have a ‘demag code’ in the GPMDB of 3 or higher.
4. The dataset must comprise site mean directions from at least 7 individual rock units (i.e. $N \geq 7$).

Datasets which passed the four criteria above are termed Group 2 here. The subset of these which also have individual site mean data with $n \geq 5$ and $k \geq 50$ have both a reasonable within-site scatter (although the definition of ‘reasonable’ is of course arbitrary) and a good number of samples with which to estimate this characteristic; they are termed Group 1.

The Groups 1 and 2 data from both time periods are summarised in Tables 2 and 3. Two NRO factors are given. *NRO factor 1* is that obtained when all the data in the set are input together grouped by the localities where they were obtained; it therefore is a measure of the amount of clustering of the data by locality rather than progressive serial correlation. *NRO factor 2* is that measured from data obtained from a stratigraphic sequence of units and therefore may reflect a gradual progression in directions. When a dataset contained more than one stratigraphic sequence, the lowest *NRO factor 2* measured is given.

These NRO factors are frequently significant (i.e. >0.95) indicating that, in a great many cases, bursts of extrusive activity caused series of lavas to record related periods of geomagnetic behaviour.

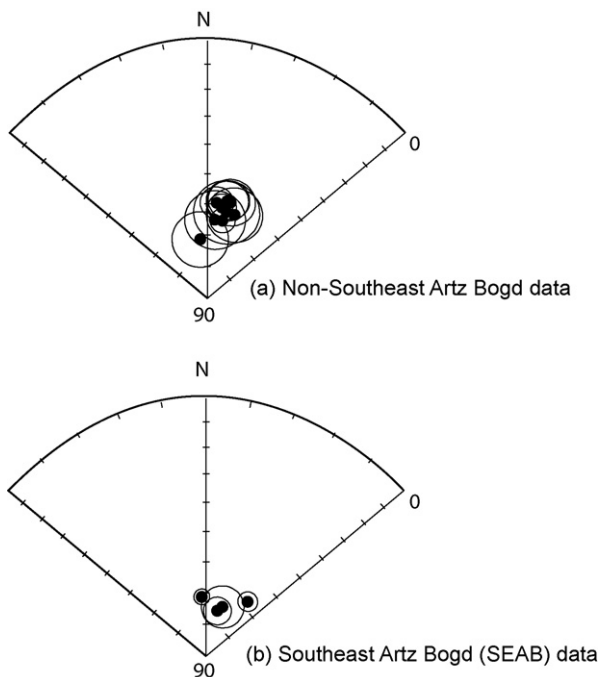


Fig. 6. Equal area plots showing the locality mean directions (and 95% confidence circles) for the Gobi Altai lavas used in this study. See Table 1 and van Hinsbergen et al. (2008) for more details.

Table 2
Group 1 datasets

| Period | Name | Reference | Age (Ma) | Rock type | Demag code | Dec (°) | Inc (°) | N | N ₀ | NRO factor 1 | NRO factor 2 | Cutoff (°) | Δ _{max} (°) | R | k | α95° | λ | S ₁ (°) | S _B (°) | S _u (°) |
|----------|-------------------------------------|-----------|----------|-------------------------------|------------|---------|---------|----|----------------|--------------|--------------|------------|----------------------|------|-------|------|-------------------|--------------------|--------------------|--------------------|
| CNS | Rajmahal Traps, India ^a | [1,2] | 113–116 | Flood basalts | 4,3 | 312.9 | –62.8 | 27 | 27 | 0.93 | 0.96 | 28.8 | 26.7 | 26.6 | 66.2 | 3.4 | –44.3 | 10.4 | 13.2 | 15.8 |
| CNS | Madagascar | [3] | 84–90 | Basalt lavas | 4 | 356.9 | –57.1 | 24 | 23 | 0.99 | 0.62 | 28.4 | 27.9 | 22.7 | 68.3 | 3.7 | –37.7 | 9.9 | 13.0 | 16.0 |
| CNS | Balantak, Indonesia ^a | [4] | 91–95 | Basalt lavas and pillows | 4 | 58.8 | –35.6 | 13 | 13 | 0.99 | 0.99 | 25.9 | 19.4 | 12.6 | 33.5 | 7.3 | –19.7 | 9.2 | 11.6 | 13.7 |
| CNS | Mt Carmel, Israel | [5] | 97 | Basalt lavas | 4 | 10.4 | 10.2 | 10 | 10 | | | 20.9 | 13.1 | 9.8 | 50.8 | 6.8 | 5.1 | 5.9 | 8.8 | 11.0 |
| CNS | Gobi Altai non-SEAB | [6,7,8] | 95–125 | Basalt lavas | 4 | 11.5 | 63.7 | 89 | 85 | 0.99 | 0.26 | 34.0 | 32.1 | 83.3 | 48.8 | 2.2 | 45.4 | 14.3 | 16.1 | 17.7 |
| CNS | Spences Bridge, Canada ^a | [9] | 104–105 | Andesitic lavas | 4 | 34.3 | 66.3 | 13 | 13 | 0.97 | 0.78 | 32.8 | 23.3 | 12.8 | 58.5 | 5.5 | 48.7 | 12.2 | 15.4 | 18.4 |
| CNS | Gobi Altai SEAB ^a | [6] | 115–119 | Basalt lavas | 4 | 9.7 | 73.4 | 25 | 25 | 0.99 | 0.41 | 28.5 | 23.7 | 24.8 | 99.8 | 2.9 | 45.4 ^b | 10.8 | 13.1 | 15.2 |
| CNS | Strand Fiord, Canada | [10] | 95 | Basalt lavas | 4 | 273.8 | 79.9 | 19 | 19 | 0.97 | 0.18 | 45.4 | 37.7 | 18.5 | 39.1 | 5.4 | 70.4 | 17.9 | 22.4 | 26.6 |
| Jurassic | Marifil, Argentina | [11] | 166–188 | Trachi-rhyolites, ignimbrites | 4 | 6.3 | –64.9 | 7 | 7 | 0.45 | | 44.5 | 41.3 | 6.8 | 33.1 | 10.6 | –46.8 | 11.4 | 22.0 | 32.2 |
| Jurassic | N El Quemado, Argentina | [11] | 154–159 | Ignimbrites, rhyolite | 4 | 5.7 | –60.0 | 12 | 12 | 0.93 | 0.86 | 34.4 | 21.1 | 11.8 | 44.1 | 6.6 | –40.9 | 13.5 | 16.4 | 18.6 |
| Jurassic | Lesotho, S Africa ^a | [12] | 175–185 | Basalt lavas | 4 | 339.3 | –54.4 | 35 | 35 | 0.99 | 0.99 | 29.3 | 28.4 | 34.3 | 47.5 | 3.6 | –34.9 | 11.2 | 13.5 | 15.8 |
| Jurassic | Camaraca, Chile | [13] | 157–174 | Andesites | 3 | 344.3 | –39.2 | 9 | 9 | 0.54 | 0.07 | 42.8 | 39.1 | 8.5 | 15.9 | 13.3 | –22.2 | 11.9 | 21.0 | 29.2 |
| Jurassic | Canelo Hills, Arizona | [14] | 149–153 | Welded tuffs | 3 | 333.8 | 30.4 | 12 | 12 | | | 30.4 | 27.0 | 11.6 | 28.6 | 8.3 | 16.3 | 8.9 | 14.1 | 18.7 |
| Jurassic | CAMP, Morocco ^a | [15] | 200 | Flood basalts | 4 | 343.5 | 42.7 | 40 | 40 | 0.99 | 0.93 | 43.3 | 39.2 | 38.0 | 19.8 | 5.2 | 24.8 | 18.3 | 21.3 | 24.2 |
| Jurassic | Hua-an, Mongolia | [16] | 146–166 | Andesites, tuff | 4 | 10.1 | 50.1 | 9 | 9 | 0.91 | | 30.2 | 26.2 | 8.8 | 45.8 | 7.7 | 30.9 | 9.4 | 14.0 | 18.7 |
| Jurassic | Manzhouli, Mongolia ^a | [16] | 146–166 | Tuffs | 4 | 30.7 | 54.3 | 13 | 12 | 0.91 | | 17.3 | 10.4 | 11.9 | 179.5 | 3.2 | 34.9 | 5.0 | 6.9 | 8.4 |

Demag code refers to that used in the Global Palaeomagnetic database (<http://www.ngu.no/dragon/Palmag/paleomag.htm>). N₀ is the number of sites before the VGP cutoff is applied. Δ_{max} is the maximum angular distance between a single pole and the mean pole after the cutoff is applied. S₁ and S_u are the upper and lower 95% confidence limits (obtained by the bootstrap method) on the VGP dispersion S_B. See text for definition of other parameters. References: [1] Tarduno et al. (2001); [2] Klootwijk (1971); [3] Risager et al. (2001); [4] Muburo et al. (1994); [5] Ron et al. (1990); [6] van Hinsbergen et al. (2008); [7,8] Hankard et al. (2005, 2007); [9] Irving and Thorkelson (1990); [10] Tarduno et al. (2002); [11] Iglesias Llanos et al. (2003); [12] Kostrov and Perrin (1996); [13] Palmer et al. (1980); [14] Kluth et al. (1982); [15] Knight et al. (2004); [16] Zhao et al. (1990).

^a The reliability of these datasets is discussed explicitly in the text.

^b The palaeolatitude of the Gobi Altai SEAB dataset was manually changed to match that of the Gobi Altai non-SEAB dataset.

However, most of the datasets have either the first or the second NRO factor less than 0.95 and this is all that is required for the dataset to provide what is likely a reasonable representation of field variations. If NRO factor 1 is low then it indicates that directions taken from different localities are not clustered suggesting that each group contains approximately the full range of geomagnetic behaviour. If NRO factor 2 is low, it indicates that at least one sampled stratigraphic section contains data that likely represents a statistically random sampling of the field.

On this basis, two Group 1 datasets present a significant risk of giving an estimate of S_B which is biased to low values—the Rajmahal Traps and Balantak. Two of the larger datasets: Lesotho and the CAMP are, together with the new Gobi Altai data (discussed in Section 4.1), clearly heavily affected by short duration bursts of volcanic activity resulting in the measurements being placed into ‘directional groups’ in the original studies (Knight et al., 2004; Kostrov and Perrin, 1996). However, in both of these cases, we suspect that the volume of data allows us to have a largely unbiased estimate of S_B.

While the Lesotho dataset produces NRO factors 1 and 2 of 0.99, the directions from these basalts pass a reversal test which suggests adequate representation of the SV; its mean pole is also within errors of other Jurassic poles for South Africa further supporting this (Kostrov and Perrin, 1996). Knight et al. (2004) split their data from the Central Atlantic Magmatic Province (CAMP) basalts in Morocco into seven directional groups, each representing a distinct spell of secular variation, which they numbered DG1 to DG7. They excluded DG4 for having reversely magnetised lavas and DG7 because it was from a unit of uncertain age and demonstrated that the overall mean direction produced by the other DG means (Dec = 344°, Inc = 41°, N = 5, k = 24.3) gave a pole indistinguishable from that of the mean pole for Africa at 200 Ma. Here we use as our dataset the combination of all the data from these same five directional groups. These produce a mean (Dec = 349°, Inc = 42°, N = 62, k = 21.2) which is very similar in direction and dispersion to the DG mean and which therefore is unlikely to be biased by over-representation of any particular period(s) of secular variation.

Welded tuffs were clearly emplaced above the Curie temperature of the ferromagnetic minerals they contain and therefore carry a spot reading of the field most likely as a thermoremanent magnetisation (TRM). Other tuff and ignimbrite units were potentially emplaced at lower temperatures which could cause them to retain a depositional remanent magnetisation (DRM) instead. If this was the case, and if layers of the pyroclastic deposits accumulated over centuries, then there is the potential for datasets containing tuffs to underestimate S_B because of averaging effects. This potential biasing effect will be discussed on a point-by-point basis in the next section.

Only two datasets – Vestfjella and Lembobo – have a significant proportion of their measurements produced from intrusive rocks. In both cases, the thicknesses of the sampled units are not given. However, their stated composition (basaltic and rhyolitic, respectively) is suggestive of them cooling rapidly which implies that they are unlikely to bias the estimate of S_B significantly through slow-cooling.

5. Results

5.1. Group 1 datasets

Fig. 7a and b summarises the results produced from Group 1 datasets for both periods. It shows that the choice of whether to use a fixed 45° cutoff or the variable cutoff developed by Vandamme (1994) makes little or no difference to the VGP dispersion curve produced in both periods.

Table 3
Group 2 datasets

| Period | Name | Refs. | Age (Ma) | Rock type | Demag code | Dec (°) | Inc (°) | N | N ₀ | NRO factor 1 | NRO factor 2 | Cutoff (°) | Δ _{max} (°) | R | k | α95° | λ | S _I (°) | S _B (°) | S _U (°) |
|----------|-------------------------------------|----------|----------|--------------------------------------|------------|---------|---------|-----|----------------|--------------|--------------|------------|----------------------|-------|-------|------|-------------------|--------------------|--------------------|--------------------|
| CNS | Mt Somers, New Zealand ^a | [17] | 92–98 | Intermediate-felsic flows and tuffs | 3 | 353.7 | −85.2 | 46 | 46 | 0.94 | | 47.3 | 46.3 | 44.6 | 31.7 | 3.8 | −80.5 | 19.9 | 23.5 | 26.8 |
| CNS | Rajmahal Traps, India ^a | [1,2] | 113–116 | Flood basalts | 4,3 | 313.5 | −62.3 | 33 | 31 | 0.93 | 0.96 | 27.9 | 27.4 | 30.6 | 70.0 | 3.1 | −43.6 | 10.1 | 12.7 | 15.1 |
| CNS | Madagascar | [3] | 84–90 | Basalt lavas | 4 | 0.3 | −59.4 | 44 | 42 | 0.99 | 0.62 | 26.2 | 24.3 | 41.5 | 79.7 | 2.5 | −40.2 | 9.6 | 11.8 | 13.8 |
| CNS | Vinita, Chile ^a | [12] | 97–106 | Intermediate lavas and tuffs | 3 | 8.0 | −55.5 | 11 | 11 | 0.66 | | 29.5 | 27.4 | 10.8 | 55.3 | 6.2 | −36.1 | 8.0 | 13.6 | 18.5 |
| CNS | Balantak, Indonesia ^a | [4] | 91–95 | Basalt lavas and pillows | 4 | 59.9 | −32.1 | 23 | 23 | | 0.99 | 26.0 | 21.8 | 22.3 | 30.4 | 5.6 | −17.4 | 9.4 | 11.7 | 14.0 |
| CNS | Mt Carmel, Israel | [5] | 97 | Basalt lavas | 4 | 10.1 | 11.9 | 11 | 11 | | | 21.2 | 13.2 | 10.8 | 43.8 | 7.0 | 6.0 | 6.4 | 9.0 | 10.8 |
| CNS | Wadi Natash, Egypt | [18] | 86–100 | Mafic to felsic lava flows | 3 | 345.4 | 16.7 | 15 | 15 | | | 26.4 | 19.7 | 14.3 | 21.4 | 8.5 | 8.5 | 8.7 | 11.9 | 14.7 |
| CNS | Gobi Altai non-SEAB | [6,7,8] | 95–125 | Basalt lavas | 4 | 11.4 | 62.8 | 129 | 116 | 0.99 | 0.26 | 33.0 | 32.0 | 113.7 | 49.6 | 1.9 | 44.2 | 14.1 | 15.6 | 17.0 |
| CNS | Spences Bridge, Canada ^a | [9] | 104–105 | Andesitic lavas | 4 | 38.5 | 64.4 | 16 | 16 | 0.97 | 0.78 | 34.8 | 23.5 | 15.6 | 42.5 | 5.7 | 46.2 | 13.5 | 16.6 | 19.2 |
| CNS | Gobi Altai SEAB ^a | [6] | 115–119 | Basalt lavas | 4 | 29.6 | 70.6 | 80 | 75 | 0.99 | 0.41 | 36.4 | 35.6 | 73.4 | 44.9 | 2.5 | 54.9 ^b | 15.4 | 17.4 | 19.4 |
| CNS | Strand Fiord, Canada | [10] | 95 | Basalt lavas | 4 | 284.8 | 80.1 | 37 | 37 | 0.97 | 0.18 | 42.7 | 37.1 | 36.2 | 43.5 | 3.6 | 70.8 | 17.8 | 20.9 | 23.9 |
| Jurassic | N El Quemado, Argentina | [11] | 154–159 | Welded ignimbrites, rhyolite | 4 | 8.9 | −60.6 | 14 | 14 | 0.93 | 0.86 | 33.7 | 22.2 | 13.7 | 45.3 | 6.0 | −41.6 | 13.8 | 15.9 | 17.9 |
| Jurassic | Marifil, Argentina | [11] | 166–188 | Trachi-rhyolites, welded ignimbrites | 4 | 2.9 | −57.0 | 11 | 10 | 0.45 | | 37.5 | 26.3 | 9.7 | 32.2 | 8.6 | −37.6 | 13.5 | 18.0 | 21.7 |
| Jurassic | Vestfjella, Antarctica ^a | [19] | 152–176 | Basaltic lavas and dykes | 3 | 31.7 | −55.6 | 26 | 24 | | | 25.2 | 25.0 | 23.6 | 56.7 | 4.0 | −36.2 | 8.0 | 11.2 | 13.9 |
| Jurassic | Lesotho, South Africa ^a | [12] | 175–185 | Basalt flows | 4 | 338.8 | −53.8 | 47 | 47 | 0.99 | 0.99 | 30.3 | 28.9 | 45.9 | 42.0 | 3.2 | −34.3 | 11.7 | 14.1 | 16.2 |
| Jurassic | Lembobo, South Africa ^a | [20] | 173–183 | Basalts & intrusive rhyolites | 3 | 336.3 | −49.3 | 21 | 17 | 0.52 | | 27.8 | 26.3 | 16.7 | 49.8 | 5.1 | −30.2 | 8.7 | 12.7 | 16.2 |
| Jurassic | Anari & Tapirapua, Brazil | [21] | 195–198 | Basalt flows | 3 | 21.2 | −46.3 | 15 | 15 | 0.52 | | 16.3 | 12.1 | 14.9 | 103.1 | 3.8 | −27.6 | 3.9 | 6.3 | 8.0 |
| Jurassic | Lepa, Argentina | [22] | 182–191 | Andesites and tuffs | 4 | 10.3 | −43.1 | 36 | 30 | 0.82 | 0.29 | 36.7 | 33.5 | 28.5 | 19.9 | 6.0 | −25.1 | 14.4 | 17.6 | 20.9 |
| Jurassic | East Elba Ophiolite, Italy | [23] | 146–157 | Pillow basalts | 3 | 199.6 | −37.9 | 10 | 10 | 0.49 | | 21.1 | 18.9 | 9.8 | 39.4 | 7.8 | −21.2 | 3.6 | 8.9 | 12.6 |
| Jurassic | Camaraca, Chile | [13] | 157–174 | Andesites | 3 | 336.2 | −35.3 | 32 | 28 | 0.54 | 0.07 | 30.0 | 29.8 | 27.0 | 27.3 | 5.3 | −19.5 | 10.8 | 13.9 | 16.8 |
| Jurassic | Coast Range Ophiolite, California | [24] | 155–165 | Pillow basalts | 3 | 40.9 | −25.4 | 10 | 10 | | | 24.7 | 19.2 | 9.8 | 38.2 | 7.9 | −13.3 | 6.2 | 11.0 | 14.5 |
| Jurassic | Lebanon | [25, 26] | 146–156 | Basalt flows and dykes, 2 tuffs | 3 | 92.2 | 15.8 | 12 | 11 | | | 20.5 | 16.3 | 10.7 | 33.4 | 8.0 | 8.1 | 4.8 | 8.6 | 11.3 |
| Jurassic | Corral Canyon, Arizona | [27] | 166–178 | Welded tuffs | 4 | 339.5 | 19.5 | 13 | 11 | | | 25.7 | 17.7 | 10.7 | 29.9 | 8.5 | 10.0 | 8.6 | 11.5 | 14.1 |
| Jurassic | Canelo Hills, Arizona | [14] | 149–153 | Welded tuffs | 3 | 337.2 | 30.1 | 15 | 14 | | | 24.0 | 18.6 | 13.7 | 41.8 | 6.2 | 16.2 | 6.8 | 10.6 | 13.2 |
| Jurassic | CAMP, Morocco ^a | [15] | 200 | Flood basalts | 4 | 349.1 | 42.3 | 64 | 63 | 0.99 | 0.93 | 41.5 | 38.5 | 60.1 | 21.3 | 4.0 | 24.5 | 17.9 | 20.3 | 22.6 |
| Jurassic | Zymoetz, Canada ^a | [28] | 190–200 | Flows, tuffs, ignimbrites | 4 | 226.3 | 48.1 | 9 | 9 | 0.24 | | 26.2 | 18.3 | 8.8 | 47.5 | 7.5 | 29.1 | 8.3 | 11.8 | 14.5 |
| Jurassic | Hua-an, Mongolia | [16] | 146–166 | Andesites, 1 tuff | 4 | 10.1 | 50.1 | 9 | 9 | 0.91 | | 30.2 | 26.2 | 8.8 | 45.8 | 7.7 | 30.9 | 9.4 | 14.0 | 18.6 |
| Jurassic | Manzhouli, Mongolia ^a | [16] | 146–166 | Tuffs | 4 | 31.7 | 54.2 | 14 | 13 | 0.91 | | 17.6 | 10.4 | 12.9 | 172.2 | 3.2 | 34.7 | 5.3 | 7.0 | 8.4 |

See Table 2 and text for definition of other parameters. References (see also Table 2): [17] Oliver et al. (1979); [18] Schult et al. (1981); [19] Løvlie (1988); [20] Henthorn, 1981; [21] Montes-Lauar et al. (1994); [22] Vizan (1998); [23] Soffel (1981); [24] McWilliams and Howell (1982); [25] Gregor et al. (1974); [26] van Dongen et al. (1967); [27] May et al. (1986); [28] Vandall and Palmer (1990).

^a The reliability of these datasets is discussed explicitly in the text.

^b The palaeolatitude of the Gobi Altai SEAB dataset was manually changed to match that of the Gobi Altai non-SEAB dataset.

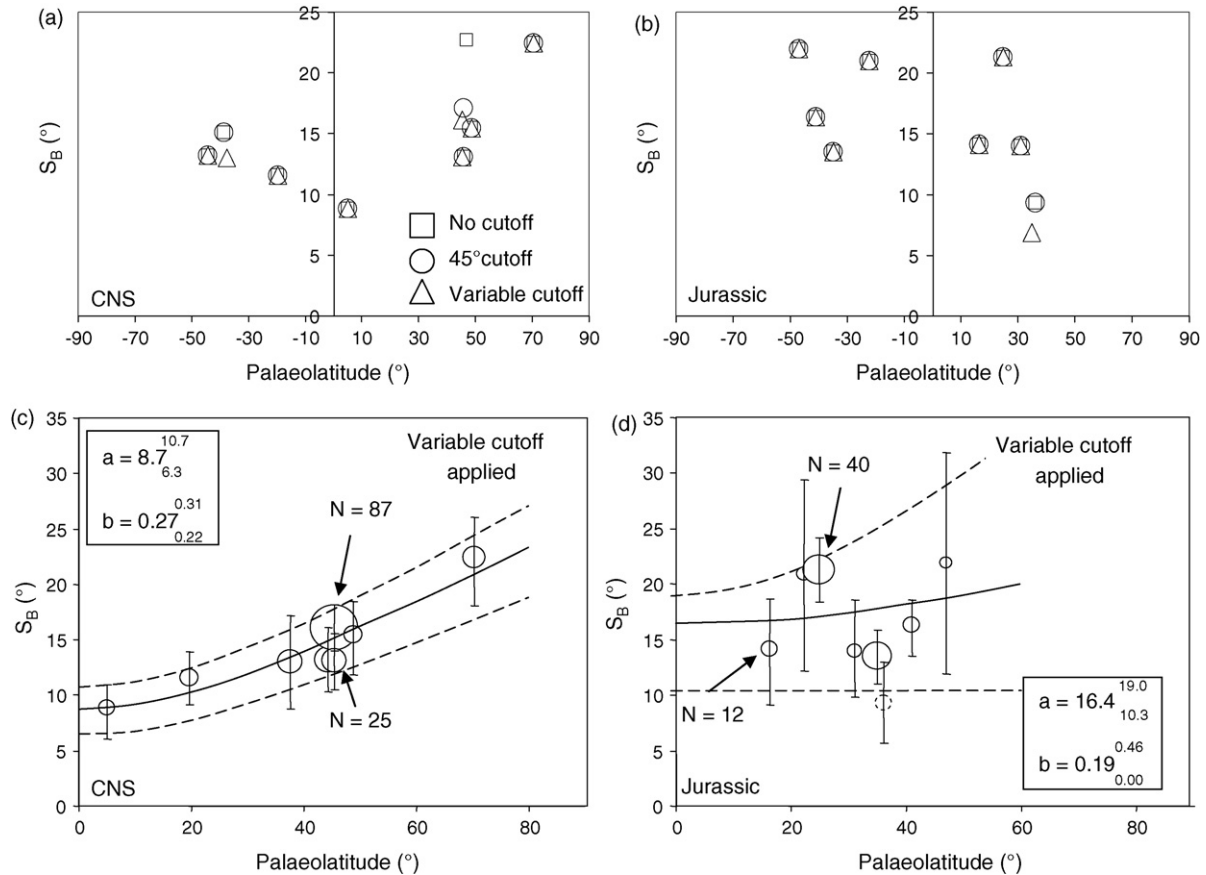


Fig. 7. Results from Group 1 ('high quality') Datasets. (a and b) The effects of three different cutoffs are shown. (c and d) The palaeolatitudes of the datasets are normalised and the size of each point relates to the size of N (a few examples are given). The shape parameters of the best-fit Model G (McFadden et al., 1988) are given with 95% bootstrap uncertainty limits and the resulting curves plotted. The dashed point in panel (d) was excluded from the Model G calculation (see text).

The datasets are far too small and few to make any meaningful test for equatorial asymmetry in the VGP dispersion recorded in both periods. However, given that Fig. 7a and b shows no obvious evidence of asymmetry and that the GAD hypothesis is normally assumed to be reasonable for these periods, we choose to plot the data from the N and S hemisphere on the same axis in Fig. 7c and d and to apply the variable VGP cutoff.

The CNS datasets appear to show rather consistent S_B - λ behaviour (Fig. 7c). In particular, at mid-latitudes we have datasets from five geographically distinct areas (three in the N and two in the S hemisphere) giving S_B values within errors of one another. One of these, the Spences Bridge dataset (with $\lambda = 48.7$) is highlighted in Tables 2 and 3 because Irving and Thorkelson (1990) noted that there was the potential for (small) errors in the correction to the palaeohorizontality. However, the good agreement of this dataset's estimate of S_B with the other four from similar palaeolatitudes suggests that this was not too serious a problem. The Balantak dataset (with $\lambda = -19.7$) has some doubts associated with its Cretaceous age (Kadarusman et al., 2004) and may instead be Tertiary. While we cannot comment on this uncertainty, we do note here that it fits the overall trend of the CNS data excellently. Similarly, the consistency displayed by the Mongolia SEAB dataset with others from a similar inferred palaeolatitude provides some support for our decision to manually adjust its value of λ (Section 4.1). Since the three datasets mentioned above do not strongly influence the fit of the Model G curve to the Group 1 data, their exclusion would only serve to unnecessarily reduce our confidence in this fit; they are therefore all retained.

The Jurassic datasets comprise little over half as much data as those in the CNS and are limited to a very short low to mid-latitude range in both hemispheres (Fig. 7d). The lowest S_B value displayed in Fig. 7b and d is from the Manzhouli dataset which comprises data taken from tuffs which gave an inconclusive result when subjected by us to the reversal test. This may indicate that the full range of SV is not represented in this dataset and that S_B is underestimated as a result. Because of this doubt and because of the strong influence it would exert, we exclude this dataset from the Model G curve fit.

Given the limitations to the Jurassic data described above, it is not possible to compare the VGP dispersion curves in Fig. 7c and 7d with any real confidence. There is a suggestion that mean S_B is lower for the low latitude sites in the CNS than in the Jurassic and that mean S_B is more dependent on palaeolatitude in the CNS. These are qualitatively the same observations as made by McFadden et al. (1991) when comparing VGP dispersion curves for their periods 80–110 and 110–195 Ma. In terms of the Model G of McFadden et al. (1988), this corresponds to the CNS data producing a lower a value and a higher b value than the Jurassic data. A more convincing observation to be made from Fig. 7 is that the values of S_B have a much less predictable relationship with palaeolatitude in the Jurassic than in the CNS. This may be only partly explained by the lower values of N for the Jurassic datasets which will tend to increase the scatter (Fig. 5) of measured S_B values.

We will now turn to the larger, lower quality datasets in Group 2 to see if these can verify the observations made above to any degree.

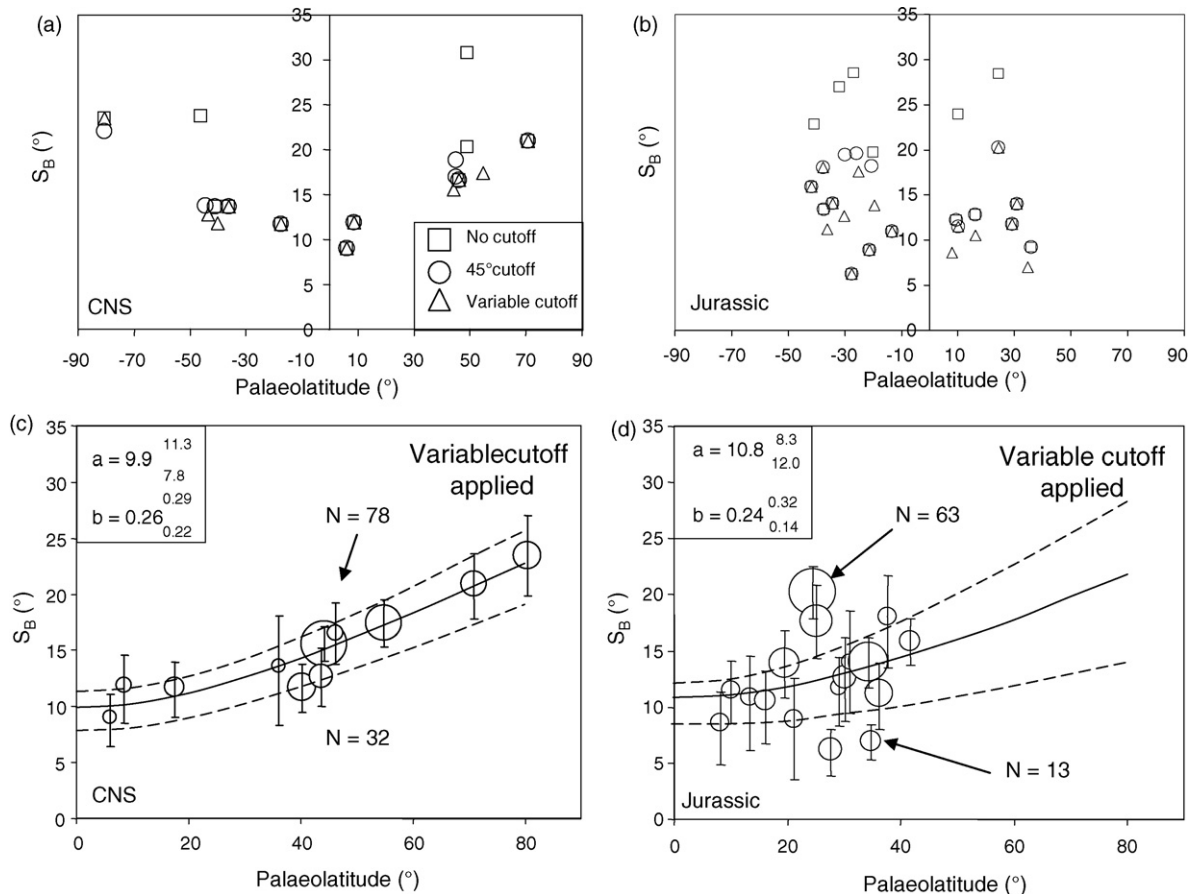


Fig. 8. Results from Group 2 ('low quality') datasets. See Fig. 7 caption for more information.

5.2. Group 2 datasets

While the choice of fixed or variable cutoff makes little difference to the CNS datasets, several of the Jurassic datasets give significantly lower values of S_B with the latter employed. Since lower quality data (in particular those with $n = 1$) are more likely to be unreliable outliers, we choose to apply the variable cutoff prescribed by Vandamme (1994) to the data in Fig. 8c and d since this is likely to be more effective at excluding them.

Fig. 8c shows that the Group 2 datasets from the CNS produce a similar VGP dispersion plot to their Group 1 equivalents and therefore verify the strong latitudinal dependence of S_B . Two Group 2 datasets (Vinita and Mt. Somers) comprise a significant number of directions from tuff units. However, both these datasets give consistent S_B values to those of others from similar palaeolatitudes and therefore do not appear to be strongly biased by time-averaging effects. Model G fitted to the Group 2 datasets has a slightly higher (though well within error) a parameter than that fitted to the Group 1 datasets which may indicate that the values of S_B in the former are marginally increased by the inclusion of poorer quality data (cf. Fig. 4c and d).

The situation for the Jurassic Group 2 datasets is not so clear-cut. They, like their Group 1 equivalents, are also rather scattered but now some mean latitudinal dependence, similar to that for the CNS data, is implied in Fig. 8d.

This newly observed relationship is not a consequence of the inclusion of non-lava data which average out PSV. While the Jurassic Lepa dataset is dominated by directions from tuffs, it has a higher than average S_B . The Zymoetz dataset which contains data from

both lavas and tuffs in unknown proportion also does not give an unusually low S_B value. Nonetheless, given the large variation in S_B values measured for the Jurassic coupled with the small palaeolatitudinal span of the datasets, we cannot rule out the apparent latitudinal dependence of mean S_B being an artefact of a few inaccurate datasets having a disproportionate weight. For example, the two datasets with the highest palaeolatitudes (North El Quemado and Marifil) are both taken from the same study and are crucial in defining the non-zero slope of the mean S_B - λ relationship.

We also note that the application of the fixed cutoff to the Group 2 Jurassic datasets produces a mean latitudinal dependence of S_B that is weaker even than that observed in Fig. 8d. A simple linear regression analysis through the VGP dispersion plots of either the variable ($R^2 = 0.086$) or the fixed ($R^2 = 0.043$) cutoff data is not significant at the 90% confidence level. Consequently, the suggested relationship in Fig. 8d is not robust.

Our analysis of Group 2 Jurassic data is inconclusive but fails to verify the comparisons of *mean* VGP dispersion behaviour made in Section 5.1 (i.e. that a is lower and b is higher in the CNS than in the Jurassic). It does, however, offer some support for the observation that S_B is much more predictable for CNS datasets than it is for Jurassic ones which itself is an interesting difference and will be discussed.

6. Discussion

We have performed a detailed analysis of PSV in the CNS and Jurassic using an updated database and with careful checking for potential sources of bias. The Groups 1 and 2 datasets are

complementary and provide a means for verifying the observations made from one another. The former datasets are most likely free from biasing effects due to palaeomagnetic measurement errors but are at increased risk of being inaccurate due to having low values of N . The Group 2 datasets, by contrast, are lower quality but both larger and more numerous. The agreement between Figs. 7c and 8c indicates that we can have some confidence in the relationship of the mean VGP dispersion with palaeolatitude shown for the CNS time period. Groups 1 and 2 datasets produce similar and similarly well-defined VGP dispersion curves indicating that this relationship is unlikely to be an artefact of either small N or small n . After examining each dataset closely, we conclude that it is also unlikely to be due to inadequate sampling of PSV (or its time averaging) by any particular datasets.

We would like to compare the pattern of mean VGP dispersion in the CNS to that in the Jurassic but this is not possible as it is not clear what the pattern in the earlier period was. The Group 1 data show a flat mean VGP dispersion curve (Fig. 7d) but this could be a product of the small values of N introducing noise; the Group 2 datasets produce an S_B - λ curve which is more similar to those of the CNS datasets but this may be due to the disproportionate influence of a few low-quality data. The uncertainty is further compounded by the severely limited palaeolatitude range of the Jurassic datasets.

Fortunately, we are not reliant on Jurassic datasets to provide a first test that average reversal frequency and PSV are related. The results of a recent analysis performed by Johnson et al. (2008) of datasets from the period 0–5 Ma (when average reversal frequency was 4.0 Myr^{-1}) are shown in Fig. 9. This analysis featured directional data with $n \geq 5$ and $k \geq 50$ in some cases and $n \geq 5$ and $k \geq 100$ in others. Consequently, their data was of at least the same reliability as the Group 1 data used in this study and far more numerous (although they also suffered from a paucity of data at high latitudes).

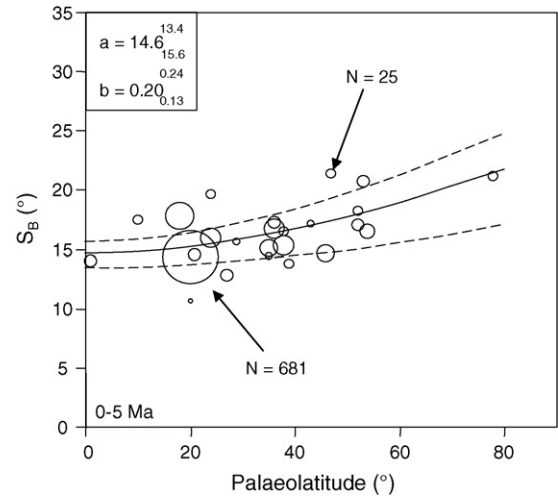


Fig. 9. Results from the study of PSV in the last 5 Myr performed by Johnson et al. (2008; data were taken from their Tables 6 and 7). The palaeolatitudes of the datasets are normalised and the size of each point relates to the size of N . The shape parameters of the best-fit Model G (McFadden et al., 1988) are given with 95% bootstrap uncertainty limits and the resulting curves plotted.

Fig. 10 compares VGP dispersion curves of binned datasets from Groups 1 and 2 data for both the CNS and the Jurassic with the binned Johnson et al. data. The 0–5 Ma data was treated using a fixed 45° cutoff rather than a variable cutoff so, for the purpose of this comparison, we treated the CNS and Jurassic data in the same way before binning them. This comparison reveals that both Groups 1 and 2 CNS curves are below the 0–5 Ma curve at low palaeolatitudes and that the overall relationship with palaeolatitude is stronger (gradient more positive) in the CNS curves.

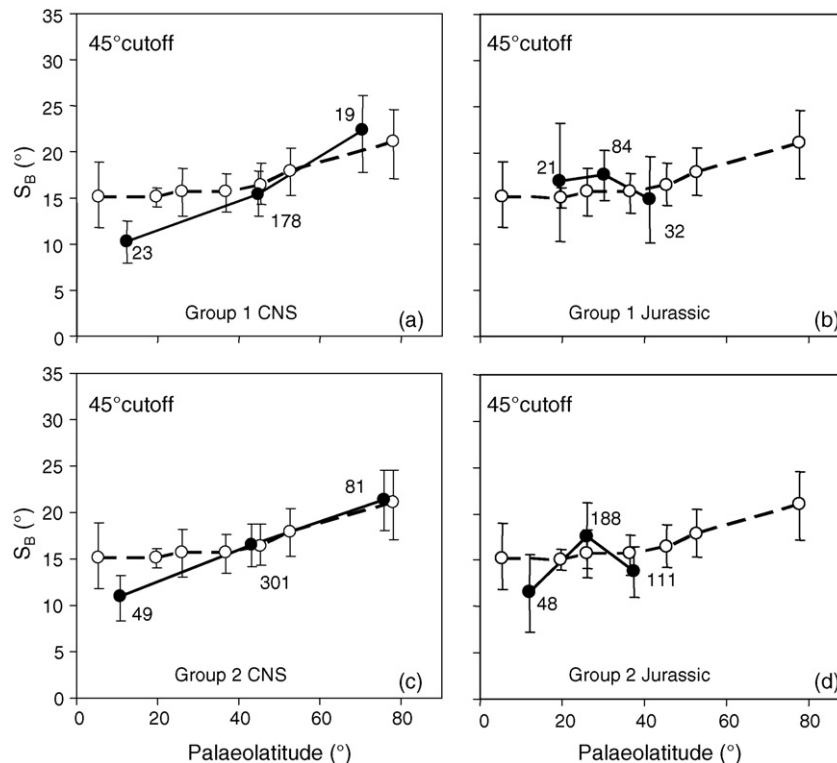


Fig. 10. VGP dispersion curves using binned data calculated using Eq. (5). Uncertainty limits were obtained by applying the same calculation to the upper and lower 95% confidence limits of the individual datasets. The dashed line shows the binned data of Johnson et al. (2008) for the last 5 Myr (same as Fig. 9). The number of site mean data in each bin is given.

As expected, the binned Group 1 Jurassic VGP dispersion curve is similar to the 0–5 Ma curve for the palaeolatitude range where there are data whereas the Group 2 Jurassic curve is more variable.

There is a potential source of bias that may have increased the estimates of S_B made in this study but which will not have affected the analysis of Johnson et al. (2008). This is the effect of errors made in the measurement of the palaeohorizontal at sampled sites. The extent of this error is extremely uncertain but is unlikely to exceed $\pm 5^\circ$ in both the strike and dip measured in most cases. This maximum error may be approximated by a Fisher-distributed scatter function (in direction space) with $k \approx 400$ which translates in pole-space to an enhanced S_B of $\sim 1^\circ$ at low latitudes and $\sim 2^\circ$ at higher latitudes. The implications of taking this source of bias into account for Fig. 10 is to slightly strengthen our conclusion that S_B is lower at low palaeolatitudes in the CNS datasets relative to the 0–5 Ma datasets and to slightly weaken our conclusion that the values of S_B in the CNS are more dependent on palaeolatitude.

Another potential source of noise for the measured values of S_B this study lies in the possibility that the original dip of volcanic units was mistaken for tectonic dip (and therefore corrected for unnecessarily). As discussed earlier (Section 4.1), this was considered to be a problem for the Mongolia SEAB dataset which we overcame by manually adjusting its inferred palaeolatitude. In general however, we would expect this to be more of a problem in intermediate to felsic units (andesites, rhyolites, ignimbrites, and tuffs) than in basalts because the higher viscosity of the former tends to produce steeper gradients. The Group 1 CNS datasets consist mostly of basalts and produces a coherent S_B – λ curve (Fig. 7c). Similar, coherent behaviour is also exhibited by the Group 2 datasets which consist of other materials. There is therefore a reasonable case to be made that the CNS datasets are unlikely to be significantly affected by this lithological problem. Unfortunately, since numerous datasets from both Groups 1 and 2 comprise data from intermediate to felsic material and since these do not display coherent behaviour in Figs. 7d and 8d, we cannot rule out that they are affected by this problem.

The Jurassic Groups 1 and 2 datasets do display a similarly high degree of scatter between their S_B datasets and we argue that this is probably not entirely due to introduced noise. For example, the CAMP and Lesotho datasets both comprise a large number of directions from basaltic flows which were inferred to have erupted at mid to low palaeolatitudes within ~ 20 Myr of one another. Yet their calculated values of S_B differ by 6 – 8° (40–60%; Tables 2 and 3). We therefore argue that the value of S_B is inherently less certain (i.e. more variable) in the Jurassic than in the CNS.

This same argument may also apply to a comparison of the 0–5 Ma and the CNS periods. Given that the average value of N for the 0–5 Ma datasets is much larger than that for the CNS datasets, we would expect the 0–5 Ma VGP dispersion curve to be much more coherent than the CNS curves (cf. Fig. 5). However, Fig. 9 indicates that this is certainly not the case which suggests that the variation of S_B with palaeolatitude may be more constant in the CNS than in the last 5 Myr also.

It therefore appears that in the CNS, the pattern of PSV was much more consistent through time than it was through the Jurassic period or even the last 5 Myr. This could be explained by periods of higher reversal frequency having a greater rate of change of PSV in time. This hypothesis appears to be supported by a study of the historical field (Hulot and Gallet, 1996) which showed that “instantaneous” VGP dispersion curves (where each dispersion value represents the longitudinal variation in the field along a line of latitude) obtained from the 1980, 1900, and 1800 fields were significantly different (see also Fig. 1b). It is also consistent

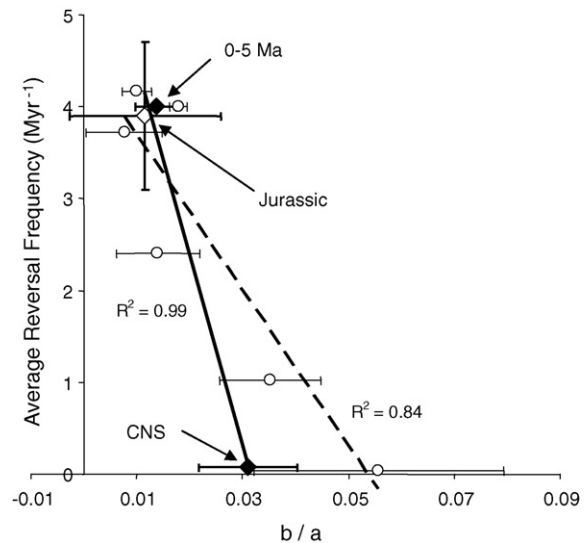


Fig. 11. The relationship between average reversal frequency and VGP dispersion curve shape. The ratio b/a refers to the shape parameters of the best-fit Model G (McFadden et al., 1988). Diamonds represent the Group 1 model fits shown in Figs. 7 and 9 and the thick line is a linear regression fit to these three points. Unfilled circles represent the curves fitted by McFadden et al. (1991) to six different periods in the last 195 Myr (see their Tables 2–7); the dashed line is a linear regression fit to these.

with the range of instantaneous VGP curves being much reduced for the Glatzmaier–Roberts Model E than for their Model G (compare the standard deviations shown by the error bars for the two VGP dispersion curves shown in Fig. 1).

The findings of this study, regarding the shapes of VGP dispersion curves from periods with different mean reversal frequencies, are (for Group 1 data at least) qualitatively similar to those reported by McFadden et al. (1991) but far more equivocal. Fig. 11 shows that there may well be a relationship between the shape of the mean VGP dispersion curve and average reversal frequency but that it is implied to be much more subtle than that reported by the previous study. Our fit of Model G to the CNS data given in McFadden et al. (1991, their Table 6) has parameters $a = 6.1$ and $b = 0.34$ while that fit to their 110–195 Ma data (their Table 7) gave $a = 18.2$ and $b = 0.14$. The differences in these parameters (particularly a) measured for the two periods was much larger for their data than for ours and it is worthwhile discussing potential reasons for this.

Firstly, we point out that the far larger and higher quality set of data used in the present study implies that its findings should be much more trustworthy. To clarify: less than 25% of the data used in this study were published at the time McFadden et al.’s database was compiled (1983) and it is possible that as much as 35% of their data did not pass our Group 1 or Group 2 criteria (they used the period 110–195 Ma instead of the Jurassic which prevents a direct comparison). Furthermore, we used more than two and a half times as much data in our study as they did in their combined period 80–195 Ma. We would expect these differences to cause the results of the present study to be less noisy and therefore less equivocal than those obtained by McFadden et al. (1991).

The fact that the opposite is true is likely to be at least partially due to McFadden et al. (1991) applying a constant S_W correction to all their data for which they did not have sufficient information to estimate it (we could not obtain their database and therefore do not know the proportion of data this entails but we expect that it was significant). For this correction, they took the median S_W value of their other lavas which was 14° (translating to a median k value of approximately 60—as an aside, it is worth noting that

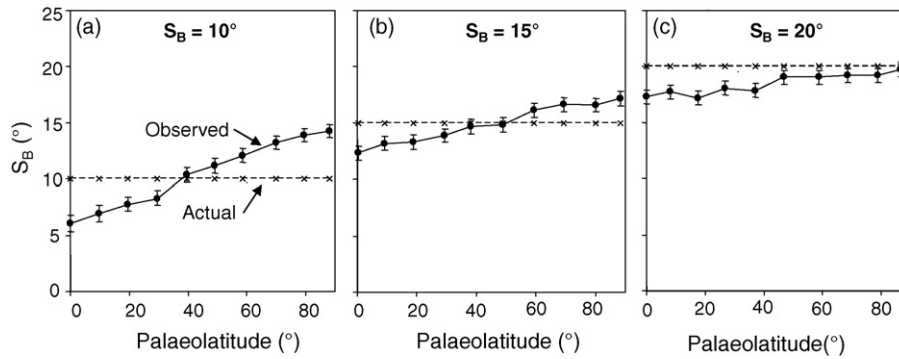


Fig. 12. VGP dispersion curves produced using simulated data treated using the same method as [McFadden et al. \(1991; filled circles\)](#) showing that their S_W correction introduces a latitudinal dependence to the plot. The true dispersion is shown by the dashed line. In all cases $N=1000$, $n=2$, and $\kappa=60$. In (c), the measured dispersions are entirely below the simulated values on account of the VGP cutoff (40°) employed.

this is much lower than our median k value of 182 which indicates the lower quality of their datasets). However, since S_W is defined in pole-space, this translates to unrealistic latitudinally dependent dispersion in direction space (k ranging from 12 for sites at the equator to 134 for sites at the poles). Note the difference between their approach and that employed by this study: we used the k value to define within-site dispersion because random errors associated with the measurement process will affect directions similarly regardless of site latitude. The consequence for their analysis is that their within-site scatter correction will have been overly large for sites with low palaeolatitude and insufficiently large for sites with high palaeolatitude.

[Fig. 12](#) shows the effect of using [McFadden et al.'s](#) approach to analyse simulated datasets with different values of (latitudinally constant) S_B . A latitudinally dependent artefact is introduced which becomes more exaggerated the smaller that the real S_B is. The effect of this artefact would be to amplify any small genuine differences in S_B . This is likely to be the main reason why [McFadden et al. \(1991\)](#) observed a much more clear-cut relationship between PSV and reversal frequency than we do. It may well also explain why they observed a strong anticorrelation between the a and b parameters of the Model G fit to their different time windows.

Although the relationship between average reversal frequency and PSV as described by VGP dispersion curves is apparently less obvious than that reported by [McFadden et al. \(1991\)](#), a relationship does appear to exist ([Fig. 11](#)) and it is qualitatively very similar to that claimed previously. This is the same conclusion ([Tarduno et al., 2002](#)) made with a smaller dataset and is important because it shows that the PSVL technique may be used, alongside or instead of magnetostratigraphy, to determine the first-order stability of the geodynamo at other times in the Earth's history. It has already been used for this purpose in studying the late Archaean–early Proterozoic geodynamo ([Biggin et al., 2008; Smirnov and Tarduno, 2004](#)) and the findings of the present study strengthen the conclusions obtained. The shape of the VGP dispersion curve produced by [Biggin et al. \(2008\)](#) implies that the geodynamo was more stable in the late Archaean–early Proterozoic than most likely at any time in the last 200 Myr. Furthermore, the high degree of consistency observed in the S_B values produced from datasets with similar palaeolatitudes implies a low rate of change of PSV pattern which is also consistent with increased dynamo stability as observed in this study.

VGP dispersion curves remain the most common and obvious means of analysing PSVL data. However, the shape of a curve is influenced by non-unique factors ([Hulot and Gallet, 1996](#)) and is not easy to interpret in physical terms. [McFadden et al. \(1988\)](#) showed that the equatorially antisymmetric spherical harmonic components of

the 1980 IGRF field model produced an instantaneous VGP dispersion curve that was zero at the equator and strongly latitudinally dependent. Conversely, the equatorially symmetric components produced a VGP dispersion curve that was more or less constant (and non-zero) with latitude.

[Hulot and Gallet \(1996\)](#) confirmed this observation for the 1900 and 1800 field models but also showed that almost all of the VGP dispersions evident in both families was produced by variations in just four components: (1,1), (2,1), (3,1), and (4,1). If the same is assumed to apply to the dynamo hundreds of millions of years ago then this might imply that variations in the equatorial dipole (1,1) and the (3,1) components were suppressed during the CNS relative to the last 5 Myr (and possibly the Jurassic as well).

7. Conclusions

1. Directional data with low n (from either igneous or sedimentary rocks) may be used to study PSV but such data should be treated cautiously (e.g. in this study, we use Group 2 data only to verify the conclusions produced from higher quality Group 1 data). When low n (even $n=1$) data is used, a within-site error correction should be estimated and applied. However, this estimate should err to low values to avoid over-correction which can significantly bias VGP dispersion curves.
2. The clear-cut relationship between PSV and mean reversal frequency observed by [McFadden et al. \(1991\)](#) for the last 195 Myr was very likely, at least in part, an artefact introduced by their analytical procedure. We expect that their application of a constant within-site scatter correction in pole-space will have tended to exaggerate small differences in their VGP dispersion curves caused by geomagnetic variations.
3. The above conclusion notwithstanding, subtle differences in VGP dispersion curves, of a qualitatively similar nature to those reported by [McFadden et al. \(1991\)](#) and [Tarduno et al. \(2002\)](#), are evident between the data collated by this study from the CNS and that collated by [Johnson et al. \(2008\)](#) for 0–5 Ma. This suggests that SV and reversal frequency are linked and that PSVL may be used as a tool to determine first-order variability in geodynamo stability.
4. A number of problems associated with the Jurassic datasets preclude any certainty about the relationship of mean VGP dispersion with palaeolatitude for this period. These datasets were frequently small in size and associated with intermediate to felsic lithologies (and therefore may have had a significant original dip); furthermore, they spanned a very limited

palaeolatitudinal range and the Groups 1 and 2 data did not produce similar S_B - λ curves. More reliable data from igneous rocks of Jurassic age, and particularly those formed at higher palaeolatitudes, are badly needed.

5. The pattern of PSV, as measured by VGP dispersion with palaeolatitude, appears to have been less time-dependent in the CNS than in both the Jurassic (but see conclusion 4 above) and the 0–5 Ma periods. This is suggestive of a relationship also observed in the Glatzmaier–Roberts dynamo model (Glatzmaier et al., 1999) whereby the reversal frequency is higher during periods when ‘instantaneous’ VGP dispersion curves are more variable in time.

Acknowledgements

This research was undertaken with funding provided by the Netherlands Science Foundation (NWO) and conducted under the programme of the Vening Meinesz Research School of Geodynamics (VMSG). Research by DJJvH was supported by UK/NERC grant NER/D/S/2003/00671 and an NWO-VENI grant. We are extremely grateful to Gary Glatzmaier for providing us with simulated data and to John Tarduno and an anonymous reviewer for comments which helped improve the manuscript.

Appendix A

See Table A1.

Table A1
New data used in this study taken from basalt lavas

| Flow | Lat (°N) | Long (°E) | Dec (°) | Inc (°) | n |
|--------------------|----------|-----------|---------|---------|---|
| Jaran Bogd | | | | | |
| 3 | 44.865 | 100.738 | 28.5 | 64.3 | 2 |
| 4 | 44.864 | 100.741 | 22.3 | 59.9 | 2 |
| 6 | 44.862 | 100.748 | 7.1 | 70.5 | 2 |
| 8 | 44.849 | 100.749 | 37.8 | 63.7 | 2 |
| 9 | 44.846 | 100.742 | 10.4 | 56.0 | 2 |
| 10 | 44.845 | 100.749 | 194.1 | 12.4 | 2 |
| 11 | 44.844 | 100.743 | 348.7 | 55.2 | 2 |
| 12 | 44.841 | 100.739 | 30.8 | 53.5 | 2 |
| 13 | 44.837 | 100.749 | 236.5 | 21.7 | 2 |
| 14 | 44.837 | 100.748 | 201.1 | 62.3 | 2 |
| 15 | 44.832 | 100.772 | 359.1 | 50.7 | 2 |
| 16 | 44.748 | 100.772 | 355.2 | 55.4 | 2 |
| 18 | 44.830 | 100.773 | 160.7 | 68.2 | 2 |
| 19 | 44.825 | 100.797 | 22.1 | 52.3 | 2 |
| Kharaat Uul | | | | | |
| KU 50 | 44.430 | 102.630 | 3.4 | 61.6 | 1 |
| KU 51 | 44.429 | 102.629 | 353.2 | 39.3 | 1 |
| KU 53 | 44.416 | 102.626 | 84.0 | 64.2 | 1 |
| KU 55 | 44.412 | 102.625 | 101.8 | 79.8 | 1 |
| KU 56 | 44.406 | 102.624 | 79.9 | 72.6 | 1 |
| KU 57 | 44.405 | 102.623 | 259.5 | 84.1 | 1 |
| KU 65 | 44.401 | 102.585 | 10.7 | 69.1 | 1 |
| KU 66 | 44.399 | 102.586 | 70.8 | 75.4 | 1 |
| KU 67 | 44.397 | 102.585 | 32.4 | 72.0 | 1 |
| KU 68 | 44.395 | 102.579 | 10.8 | 73.7 | 1 |
| KU 69 | 44.393 | 102.578 | 21.0 | 65.3 | 1 |
| KU 71 | 44.386 | 102.581 | 44.6 | 67.7 | 1 |
| KU 72 | 44.383 | 102.581 | 64.9 | 76.4 | 1 |
| KU 73 | 44.377 | 102.583 | 53.5 | 59.2 | 1 |
| KU 74 | 44.370 | 102.623 | 11.4 | 47.2 | 1 |
| KU 75 | 44.372 | 102.634 | 47.8 | 58.4 | 1 |
| KU 76 | 44.372 | 102.635 | 67.4 | 53.6 | 1 |
| KU 77 | 44.374 | 102.648 | 343.0 | 67.8 | 1 |
| KU 78 | 44.372 | 102.649 | 16.7 | 65.5 | 1 |
| KU 79 | 44.371 | 102.650 | 47.0 | 73.0 | 1 |
| KU 80 | 44.371 | 102.650 | 77.7 | 58.8 | 1 |
| KU 81 | 44.370 | 102.657 | 55.9 | 66.6 | 1 |
| KU 83 | 44.368 | 102.683 | 27.0 | 66.4 | 1 |

Table A1 (Continued)

| Flow | Lat (°N) | Long (°E) | Dec (°) | Inc (°) | n |
|--------|----------|-----------|---------|---------|---|
| KU 84 | 44.367 | 102.684 | 76.0 | 57.1 | 1 |
| KU 85 | 44.367 | 102.684 | 49.3 | 65.1 | 1 |
| KU 87 | 44.365 | 102.698 | 32.8 | 69.7 | 1 |
| KU 90 | 44.358 | 102.705 | 354.0 | 67.1 | 1 |
| KU 92 | 44.351 | 102.704 | 27.3 | 63.7 | 1 |
| KU 93 | 44.350 | 102.703 | 15.0 | 66.3 | 1 |
| KU 94 | 44.348 | 102.703 | 88.5 | 78.1 | 1 |
| KU 95 | 44.347 | 102.704 | 67.1 | 81.8 | 1 |
| KU 96 | 44.344 | 102.707 | 50.5 | 61.6 | 1 |
| KU 97 | 44.343 | 102.808 | 18.6 | 64.5 | 1 |
| KU 98 | 44.342 | 102.709 | 127.6 | 72.2 | 1 |
| KU 99 | 44.339 | 102.712 | 5.3 | 72.1 | 1 |
| KU 100 | 44.340 | 102.716 | 292.4 | 80.3 | 1 |
| KU 101 | 44.339 | 102.718 | 48.3 | 77.2 | 1 |
| KU 102 | 44.339 | 102.720 | 34.2 | 61.7 | 1 |
| KU 103 | 44.338 | 102.728 | 48.3 | 53.7 | 1 |
| KU 104 | 44.337 | 102.740 | 73.9 | 70.8 | 1 |
| KU 105 | 44.337 | 102.740 | 36.1 | 67.5 | 1 |
| KU 106 | 44.336 | 102.741 | 47.8 | 60.8 | 1 |
| KU 107 | 44.334 | 102.751 | 39.0 | 64.9 | 1 |
| KU 109 | 44.331 | 102.756 | 102.8 | 54.6 | 1 |
| KU 110 | 44.331 | 102.758 | 9.0 | 64.4 | 1 |
| KU 111 | 44.330 | 102.760 | 7.9 | 64.9 | 1 |
| KU 112 | 44.330 | 102.764 | 28.2 | 68.6 | 1 |
| KU 113 | 44.329 | 102.766 | 16.2 | 63.9 | 1 |
| KU 115 | 44.304 | 102.774 | 25.7 | 54.9 | 1 |
| KU 116 | 44.302 | 102.775 | 17.3 | 61.3 | 1 |
| KU 118 | 44.296 | 102.773 | 56.7 | 71.7 | 1 |
| KU 119 | 44.293 | 102.772 | 1.5 | 60.7 | 1 |
| KU 120 | 44.292 | 102.771 | 52.1 | 65.4 | 1 |
| KU 121 | 44.289 | 102.774 | 59.0 | 67.0 | 1 |

All directions are tilt-corrected.

References

- Biggin, A.J., Strik, G., Langereis, C.G., 2008. Evidence for a very long-term-trend in geomagnetic secular variation. *Nature Geoscience* 1, 395–398.
- Biggin, A.J., Thomas, D.N., 2003. Analysis of long-term variations in the geomagnetic poleoidal field intensity and evaluation of their relationship with global geodynamics. *Geophysical Journal International* 152 (2), 392–415.
- Courillot, V., Olson, P., 2007. Mantle plumes link magnetic superchrons to Phanerozoic mass depletion events. *Earth and Planetary Science Letters* 260, 495–504.
- Cox, A., 1970. Latitudinal dependence of the angular dispersion of the geomagnetic field. *Geophysical Journal of the Royal Astronomical Society* 20, 253–269.
- Cronin, M., Tauxe, L., Constable, C., Selkin, P., Pick, T., 2001. Noise in the quiet zone. *Earth and Planetary Science Letters* 190 (1–2), 13–30.
- Fisher, R.A., 1953. Dispersion on a sphere. *Proceedings of the Royal Society of London* A217, 295–305.
- Glatzmaier, G.A., Coe, R.S., Hongre, L., Roberts, P.H., 1999. The role of the Earth's mantle in controlling the frequency of geomagnetic reversals. *Nature* 401 (6756), 885–890.
- Glatzmaier, G.A., Roberts, P.H., 1995. A 3-dimensional self-consistent computer-simulation of a geomagnetic-field reversal. *Nature* 377 (6546), 203–209.
- Gong, Z., Langereis, C.G., Mullender, T.A.T., 2008. The rotation of Iberia during the Aptian and the opening of the Bay of Biscay. *Earth and Planetary Science Letters*, doi:10.1016/j.epsl.2008.06.016.
- Gradstein, F.M., Ogg, J.G., Smith, A.G. (Eds.), 2004. *A Geologic Time Scale 2004*. Cambridge University Press, Cambridge, 589 pp.
- Gregor, C.B., Mertzman, S., Nairn, A.E.M., Negendank, J., 1974. The paleomagnetism of some Mesozoic and Cenozoic volcanic rocks from the Lebanon. *Tectonophysics* 21, 375–395.
- Gubbins, D., 1994. Geomagnetic polarity reversals—a connection with secular variation and core–mantle interaction. *Reviews of Geophysics* 32 (1), 61–83.
- Gubbins, D., 1999. The distinction between geomagnetic excursions and reversals. *Geophysical Journal International* 137 (1), F1–F3.
- Hankard, F., Cogne, J.P., Kravchinsky, V., 2005. A new Late Cretaceous paleomagnetic pole for the west of Amuria block (Khunnen Uul, Mongolia). *Earth and Planetary Science Letters* 236 (1–2), 359–373.
- Hankard, F., Cogne, J.P., Quidelleur, X., Bayasgalan, A., Lkhagvadorj, P., 2007. Palaeomagnetism and K–Ar dating of Cretaceous basalts from Mongolia. *Geophysical Journal International* 169, 898–908.
- Henthorn, D.I., 1981. The magnetostratigraphy of the Lebombo Group along the Olifants River, Kruger National Park. *Annals of the Geological Survey of South Africa* 15, 1–10.
- Hulot, G., Gallet, Y., 1996. On the interpretation of virtual geomagnetic pole (VGP) scatter curves. *Physics of the Earth and Planetary Interiors* 95 (1–2), 37–53.

- Iglesia Llanos, M.P.I., et al., 2003. Palaeomagnetic study of the El Quemado complex and Marifil formation, Patagonian Jurassic igneous province, Argentina. *Geophysical Journal International* 154 (3), 599–617.
- Irving, E., Thorkelson, D.J., 1990. On determining paleohorizontal and latitudinal shifts—Paleomagnetism of Spences Bridge Group, British-Columbia. *Journal of Geophysical Research—Solid Earth and Planets* 95 (B12), 19213–19234.
- Jackson, A., Jonkers, A.R.T., Walker, M.R., 2000. Four centuries of geomagnetic secular variation from historical records. *Philosophical Transactions of the Royal Society of London Series a—Mathematical Physical and Engineering Sciences* 358 (1768), 957–990.
- Johnson, C.L., et al., 2008. Recent investigations of the 0–5 Ma geomagnetic field recorded by lava flows. *Geochemistry Geophysics Geosystems* 9, Q04032, doi:10.1029/2007GC001696.
- Kadarusman, A., Miyashita, S., Maruyama, S., Parkinson, C.D., Ishikawa, A., 2004. Petrology, geochemistry and paleogeographic reconstruction of the East Sulawesi Ophiolite, Indonesia. *Tectonophysics* 392 (1–4), 55–83.
- Klootwijk, C.T., 1971. Palaeomagnetism of the Upper Gondwana–Rajmahal Traps, NE India. *Tectonophysics* 12, 449–467.
- Kluth, C.F., Butler, R.F., Harding, L.E., Shafiqullah, M., Damon, P.E., 1982. Paleomagnetism of late Jurassic rocks in the Northern Canelo Hills, Southeastern Arizona. *Journal of Geophysical Research* 87, 7079–7086.
- Knight, K.B., et al., 2004. The central Atlantic magmatic province at the Triassic–Jurassic boundary: paleomagnetic and Ar-40/Ar-39 evidence from Morocco for brief, episodic volcanism. *Earth and Planetary Science Letters* 228 (1–2), 143–160.
- Kosterov, A.A., Perrin, M., 1996. Paleomagnetism of the Lesotho basalt, southern Africa. *Earth and Planetary Science Letters* 139 (1–2), 63–78.
- Kruiver, P.P., Dekkers, M.J., Langereis, C.G., 2000. Secular variation in Permian red beds from Dome de Barrot, SE France. *Earth and Planetary Science Letters* 179 (1), 205–217.
- Larson, R.L., Olson, P., 1991. Mantle plumes control magnetic reversal frequency. *Earth and Planetary Science Letters* 107 (3–4), 437–447.
- Lee, S., 1983. A study of the time-averaged palaeomagnetic field for the last 195 million years. Ph.D. Thesis, Australian National University, Canberra.
- Løvlie, R., 1988. Evidence for Deuteric Magnetization in Hydrothermally Altered Mesozoic Basaltic Rocks from East Antarctica. *Physics of the Earth and Planetary Interiors* 52 (3–4), 352–364.
- May, S.R., Butler, R.F., Shafiqullah, M., Damon, P.E., 1986. Paleomagnetism of Jurassic volcanic rocks in the Patagonia mountains, southeastern Arizona: implications for the North American 170 Ma reference pole. *Journal of Geophysical Research* 91, 11545–11555.
- McElhinny, M.W., McFadden, P.L., 1997. Palaeosecular variation over the past 5 Myr based on a new generalized database. *Geophysical Journal International* 131 (2), 240–252.
- McFadden, P.L., Merrill, R.T., 1993. Inhibition and geomagnetic-field reversals. *Journal of Geophysical Research—Solid Earth* 98 (B4), 6189–6199.
- McFadden, P.L., Merrill, R.T., McElhinny, M.W., 1988. Dipole quadrupole family modeling of paleosecular variation. *Journal of Geophysical Research—Solid Earth and Planets* 93 (B10), 11583–11588.
- McFadden, P.L., Merrill, R.T., McElhinny, M.W., Lee, S.H., 1991. Reversals of the Earth's magnetic-field and temporal variations of the dynamo families. *Journal of Geophysical Research—Solid Earth and Planets* 96 (B3), 3923–3933.
- McWilliams, M.O., Howell, D.G., 1982. Exotic terranes of western California. *Nature* 297, 215–217.
- Merrill, R.T., McFadden, P.L., 2003. The geomagnetic axial dipole field assumption. *Physics of the Earth and Planetary Interiors* 139 (3–4), 171–185.
- Montes-Lauar, C.R., et al., 1994. The Anari and Tapirapua–Jurassic Formations, Western Brazil—Paleomagnetism. *Geochemistry and Geochronology, Earth and Planetary Science Letters* 128 (3–4), 357–371.
- Mubroto, B., Briden, J.C., McClelland, E., Hall, R., 1994. Paleomagnetism of the Balantak Ophiolite, Sulawesi. *Earth and Planetary Science Letters* 125 (1–4), 193–209.
- Ogg, J.G., 2004. The Jurassic period. In: Gradstein, F.M., Ogg, J.G., Smith, A.G. (Eds.), *A Geological Time Scale 2004*. Cambridge University Press, Cambridge, pp. 307–339.
- Ogg, J.G., Smith, A.G., 2004. The geomagnetic polarity time scale. In: Gradstein, F.M., Ogg, J.G., Smith, A.G. (Eds.), *A Geological Time Scale 2004*. Cambridge University Press, Cambridge, pp. 63–86.
- Oliver, P.J., Mummie, T.C., Grindley, G.W., Vella, P., 1979. Paleomagnetism of the upper Cretaceous Mount Somers Volcanics, Canterbury, New Zealand. *New Zealand Journal of Geology and Geophysics* 22, 199–212.
- Opdyke, N.D., Channell, J.E.T., 1996. *Magnetic Stratigraphy*. Academic Press, London, 346 pp.
- Palmer, H.C., Hayatsu, A., MacDonald, W.D., 1980. The middle Jurassic Camarca Formation, Arica, Chile: palaeomagnetism, K–Ar age dating and tectonic implications. *Geophysical Journal of the Royal Astronomical Society* 62, 155–172.
- Prevot, M., Derder, M.E., McWilliams, M., Thompson, J., 1990. Intensity of the Earth's magnetic-field—evidence for a Mesozoic Dipole Low. *Earth and Planetary Science Letters* 97 (1–2), 129–139.
- Riisager, J., Perrin, M., Riisager, P., Vandamme, D., 2001. Palaeomagnetic results and palaeointensity of Late Cretaceous Madagascar basalt. *Journal of African Earth Sciences* 32 (3), 503–518.
- Ron, H., Nur, A., Hofstetter, A., 1990. Late Cenozoic and recent strike slip tectonics in Mt. Carmel, Northern Israel. *Annales Tectonicae* 4 (70–80).
- Schult, A., Hussain, A.G., Soffel, H.C., 1981. Paleomagnetism of upper Cretaceous volcanics and Nubian Sandstones of Wadi Natash, SE Egypt and implications for the polar wander path for Africa in the Mesozoic. *Journal of Geophysics* 50, 16–22.
- Smirnov, A.V., Tarduno, J.A., 2004. Secular variation of the Late Archean Early Proterozoic geodynamo. *Geophysical Research Letters* 31 (16), doi:10.1029/2004GL020333.
- Soffel, H.C., 1981. Palaeomagnetism of a Jurassic ophiolite series in east Elba (Italy). *Journal of Geophysics* 49, 1–10.
- Tarduno, J.A., Cottrell, R.D., Smirnov, A.V., 2001. High geomagnetic intensity during the Mid-Cretaceous from Thellier analyses of single plagioclase crystals. *Science* 293 (5530), 607–1607.
- Tarduno, J.A., Cottrell, R.D., Smirnov, A.V., 2002. The Cretaceous superchron geodynamo: observations near the tangent cylinder. *Proceedings of the National Academy of Sciences of the United States of America* 99 (22), 14020–14025.
- Tarduno, J.A., et al., 2003. The Emperor Seamounts: Southward motion of the Hawaiian hotspot plume in earth's mantle. *Science* 301 (5636), 1064–1069.
- Tauxe, L., Hartl, P., 1997. 11 million years of Oligocene geomagnetic field behaviour. *Geophysical Journal International* 128, 217–229.
- Tauxe, L., Staudigel, H., 2004. Strength of the geomagnetic field in the Cretaceous Normal Superchron: new data from submarine basaltic glass of the Troodos Ophiolite. *Geochemistry Geophysics Geosystems* 5 (Art. No. Q02H06).
- Thomas, D.N., Biggin, A.J., Schmidt, P.W., 2000. A palaeomagnetic study of Jurassic intrusives from southern New South Wales: further evidence for a pre-Cenozoic dipole low. *Geophysical Journal International* 140 (3), 621–635.
- van Dongen, P.G., van der Voo, R., Raven, T., 1967. Paleomagnetic research in the Central Lebanon Mountains and in the Tartous area (Syria). *Tectonophysics* 4, 35–53.
- van Hinsbergen, D.J.J., Straathof, G.B., Kuiper, K.F., Cunningham, W.D., Wijbrans, J., 2008. No vertical axis rotations during Neogene transpressional orogeny in the NE Gobi Altai: coinciding Mongolian and Eurasian early Cretaceous apparent polar wander paths. *Geophysical Journal International* 173, 105–126.
- Vandall, T.A., Palmer, H.C., 1990. Canadian cordilleran displacement—paleomagnetic results from the early Jurassic Hazelton Group, Terrane-I, British-Columbia, Canada. *Geophysical Journal International* 103 (3), 609–619.
- Vandamme, D., 1994. A new method to determine paleosecular variation. *Physics of the Earth and Planetary Interiors* 85 (1–2), 131–142.
- Vizan, H., 1998. Paleomagnetism of the Lower Jurassic Lepa and Osta Arena formations, Argentine Patagonia. *Journal of South American Earth Sciences* 11 (4), 333–350.
- Watson, G.S., Beran, R.J., 1967. Testing a sequence of unit vectors for serial correlation. *Journal of Geophysical Research* 72, 5655–5659.
- Zhao, X.X., Coe, R.S., Zhou, Y.X., Wu, H.R., Wang, J., 1990. New paleomagnetic results from Northern China—collision and suturing with Siberia and Kazakhstan. *Tectonophysics* 181 (1–4), 43–81.